An assessment of nitrogen dioxide (NO_2) and ozone (O_3) distribution in Edmonton, Canada employing remote sensing data (2018 – 2023)

By
Md Moniruzzaman

A Thesis Submitted to
Saint Mary's University, Halifax, Nova Scotia
in Partial Fulfillment of the Requirements for
the Degree of Master of Arts in Geography.

December, 2024, Halifax, Nova Scotia

Approved: Dr. Mathew Novak
(Supervisor)

Approved: Dr. Patricia Matsumoto
(Committee Member)

Approved: Dr. Peter Bush
(External Examiner)

Date: December, 2024

An assessment of nitrogen dioxide (NO_2) and ozone (O_3) distribution in Edmonton, Canada employing remote sensing data (2018 – 2023)

by Md Moniruzzaman

Abstract

This study analyzes the temporal and spatial distribution of satellite-observed NO_2 and O_3 concentrations in Edmonton, Canada, from July 2018 to June 2023. It explores the relationship of NO_2 and O_3 concentrations with elevation, temperature, road density, and population density. Results show higher NO_2 concentrations during winter and lower in fall months; however, O_3 concentrations remain relatively stable compared to NO_2 during the study period. NO_2 concentrations are highest in central Edmonton and lowest in surrounding suburban regions, while O_3 shows higher concentrations in central and western Edmonton and lower in eastern and southern suburban areas. Higher NO_2 concentrations are found on Wednesdays and lower on Sundays while O_3 remains consistent throughout the week. The research methodology adopted in this study may help the scientific community understand the complex interactions between anthropogenic activities and air pollution. Furthermore, the findings may help guide urban planners and policy makers in prioritizing air pollution control in the hotspot areas identified in the study.

December, 2024

Table of Contents

List of Tables

List of Figures

Chapter 1 Introduction

1.1 Background of the Study

The global urban population is increasing rapidly, triggering a variety of urban problems including land degradation, housing affordability, and traffic congestion among many others. Urban air pollution is a notable issue arising from rapid development, causing 4.2 million premature deaths each year (World Health Organization, 2021). The Global Burden of Disease (GBD) project identifies air pollution as the 5th leading cause of mortality worldwide, causing 8.7% (or 4.9 million) premature deaths in 2017 (Health Canada, 2021; IHME, 2019).

Canada's population is growing, which increases the demand for food, housing, transportation, and importantly daily necessary goods and services (Statistics Canada, 2022a). All are key drivers of air pollution. Air pollution has a diverse impact on Canadians, including 17,400 premature deaths and annual healthcare costs of $146 billion in 2018 (Health Canada, 2024a). Additionally, traffic-related air pollution in Canada contributes to 1,200 premature deaths and costs healthcare $9.5 billion annually (Health Canada, 2024b). Health Canada finds that these premature deaths and other adverse health impacts in Canada are associated with the increase in ambient concentrations of nitrogen dioxide (NO_2), ozone (O_3), and fine particulate matter $PM_{2.5}$ (Health Canada, 2024b). These pollutants can be influenced by human activities such as fuel combustion and industrial processes, as well as emissions from natural events like wildfires.

Considering the present need for better monitoring of air pollutants, the current research aims to study key air pollutants for five consecutive years starting from July 1st 2018 – June 30th 2023 in the city of Edmonton, Canada. According to the World Health Organization (WHO), five major air pollutants have diverse health impacts: nitrogen oxide (NO_x), sulfur oxides (SOx),

ozone (O_3), particulate matter (PM), and carbon monoxide (CO) (World Health Organization, 2021, 2024). Generally, air pollutants subdivide into two classes: primary air pollutants directly emitted from a source, (e.g. NO_2, SO_2); and secondary air pollutants where primary air pollutants react in the atmosphere, (e.g. O_3, H_2O_2). Among them, NO_2 is the most serious health concern (Correaa et al., 2022; Goshua et al., 2022). While short-lived, NO_2 is a primary precursor of O_3, particulate matter (PM), and the most important contributor to acid rain (Health Canada, 2021). At the provincial and territorial level, Alberta emits the highest NO_x in 2022. In 2022, among provinces and territories, Alberta accounted for 40% of the national NO_x emissions, much of this stemming from the Oil and Gas industry (Environment and Climate Change Canada, 2024). Across Canada, the largest and second-largest contributors to NO_x emissions are the oil and gas industry (increased by 29%) and the transportation (road, rail, air, and marine) sector (representing 28% of total national emissions) between 1990 and 2022 (Environment and Climate Change Canada, 2024).

O_3 accumulation is also of great concern, causing premature deaths, chronic blockages, asthma, and pulmonary disorders (Bălă et al., 2021; Health Canada, 2021). Apart from health impacts, O_3 harms vegetation and ecosystems by disrupting the ability of plants to open their microscopic leaf pores for respiration, and higher O_3 concentrations decrease agricultural crop and commercial forest yields (IOWA Department of Natural Resources, 2024; National Park Service, 2024). Importantly, most of the tropospheric level O_3 occurs due to the photochemical reactions of NO_2 (Ganzeveld et al., 2010; Valacchi et al., 2004). Therefore, both NO_2 and O_3 pollutants were chosen for the present study.

Canada has six cities with populations over one million: Toronto (ON), Montreal (QC), Vancouver (BC), Calgary (AB), Edmonton (AB), and Ottawa-Gatineau (ON) (Statistics Canada,

2022a). Among all, Edmonton and Calgary have experienced the highest and 2nd highest population growth by 20% and 19.2% from 2011 – 2021 respectively (Statistics Canada, 2022a). Compared to Calgary, Edmonton has more ground-based pollution monitoring station data available within the population centre boundary, and the stations are well distributed throughout the study area. Edmonton is the most populous northern city on the continent, having a population density of more than 1,800 population density per km^2, and is less influenced by air pollution from surrounding cities (Statistics Canada, 2022a). For these reasons, Edmonton was chosen as a study area for the present research work.

1.2 Research Questions

The study explores two specific research questions, specifically:

1. What are the spatial and temporal distribution of NO_2 and O_3 across Edmonton city from July 2018 to June 2023?
2. How do elevation, temperature, road density, and population density correlate with NO_2 and O_3 across Edmonton City?

Remote sensing is the primary data source for interrogating these questions. The data is collected through satellites and is one of the leading sources for measuring, monitoring, visualizing, and managing air pollutants on a global, regional, national, and neighborhood scale. It also provides synoptic datasets with global coverage (at different spatial resolutions) and a wide range of temporal datasets i.e., hourly, daily, monthly, and annual. Satellite-derived air pollution and climate data are generally freely available in several open-source platforms such as Google Earth Engine (GEE), Copernicus Open Access Hub, Giovanni of Earth Data, etc. (European Space Agency, 2023a; Google Earth Engine, 2024a; NASA, 2024). European Space Agency operated Sentinel-5 Precursor (Sentinel-5P) provides the highest resolution air pollution

data products and is freely available (European Space Agency, 2023b). Hence, the study utilizes Sentinel-5P datasets for the present research.

Sentinel-5P passes twice a day over the Edmonton city. That means two raster images for a day for one pollutant (NO_2/O_3). So, for five consecutive years, it requires 3,650 (5 X 365 X 2) images to study one pollutant (NO_2/O_3), and to study two pollutants (NO_2 and O_3), requires a total of 7,300 (3650 X 2) images. To acquire this huge amount of satellite images and manage them in the desktop computing environment is challenging, so the study employs the GEE platform for its computation capacities on the cloud platform. GEE is an emerging web-based API platform for geospatial data collection, processing, analysis, visualization, and extract outputs in desired formats (Google Earth Engine, 2024a). The Sentinel-5P datasets are used to assess the spatial and temporal distribution of NO_2 and O_3.

Furthermore, the study incorporates four explanatory variables to try to understand what may contribute to different concentrations of NO_2 and O_3 across the city: digital elevation model (DEM) (referred to as elevation), temperature (at 2m), road density, and population density to explain the patterns of NO_2 and O_3.

1.3 Structure of the Research

The following thesis on "Temporal and spatial distribution of NO_2 and O_3 concentrations in Edmonton, Canada employing remote sensing data" has been carried out with six chapters. The structure of the research is as follows:

Chapter 1 describes the background of the study, research questions, and the structure of the research.

Chapter 2 comprises the theoretical background of research with relevant concepts, terminologies, tools, and techniques along with a literature review.

Chapter 3 briefly describes the study area, lists of used data and materials, and methods adopted to conduct the research work.

Chapter 4 presents the results of the study, including spatial and temporal patterns of NO_2 and O_3 concentration, hotspot analysis, and relationships with explanatory variables.

Chapter 5 briefly describes the results with associated facts referring to other published work and illustrates data-related issues.

Chapter 6 describes the summary of the research and the scope of future work.

Chapter 2 Literature Review

A thorough survey of relevant literature related to air pollution research, particularly on nitrogen dioxide (NO_2) and ozone (O_3), their impacts, and the methodology adopted by researchers, has been performed for the present study. The air pollution problem has been studied in different parts of the world from different perspectives using unique methodological frameworks. The studies on air pollution measuring and monitoring using satellite measurements and station observations have an established history, becoming more advanced and specialized. Many studies related to this field have been referred to here, to understand the issue and its different dimensions. The literature review aims to provide an overview of the current state of knowledge on air pollutants, their impact, and methods adopted by other researchers to analyze pollutants.

2.1 Air Pollution

Primarily, air pollution refers to the presence of harmful substances, such as ozone (O_3), nitrogen dioxide (NO_2), and other pollutants, in various atmospheric layers (e.g., troposphere, stratosphere). There are two main sources of these pollutants: (a) natural sources, such as wildfires or volcanic eruptions, and (b) human activities, such as transportation, industrial processes, energy production, and household uses (e.g., oils and natural gas to heat homes) (Amin et al., 2017; National Institute of Environmental Health Sciences, 2023). Many pollutants undergoes various chemical transformations in the atmosphere and can travel long distances, which has a greater impact on air quality at different scales, e.g., local, regional scale, and global scaless (Seinfeld & Pandis, 2016).

Air pollutants can be categorized into two major classes: primary pollutants and secondary pollutants. Primary air pollutants like NO_2, SO_2, etc., are directly emitted from sources such as

vehicles and industrial infrastructure (European Space Agency, 2023b, 2024; Seinfeld & Pandis, 2016). Secondary air pollutants like O_3, form through a chemical reaction in the atmosphere by interacting with other primary air pollutants or with other particles and catalyzed by sunlight (European Space Agency, 2024; Lu, 2022; Monks et al., 2015). NO_2 is one of the key air pollutants that are short-lived and of serious health concern, according to Correaa et al. (2022) and Goshua et al. (2022) (Correaa et al., 2022; Goshua et al., 2022). Moreover, NO_2 is a major source of O_3, particulate matter (PM), and primarily causes acid rain according to Health Canada, 2021 (Health Canada, 2021).

2.2 Fundamentals of NO_2 and O_3

Most commonly, NO_2 is generated by combustion, including vehicular emissions, industrial processes, residential heating, and cooking. Vehicular emissions, particularly diesel engines are a major source of NO_2 (Wallington et al., 2022). Nitrogen oxides (NO_x) comprised of both NO and NO_2 are a by-product of burning fossil fuels in internal combustion engines, NO_2 is formed by the reaction of NO with O_2 in the atmosphere (Atkinson, 2000). Power plants, oil refineries, and other industrial activities that are dependent on the combustion of fossil fuels such as coal, oil, and gas, emits significant amounts of NO_x (Leue et al., 2001). Again, burning these fuels at elevated temperatures produces NOx, afterwords NO_x transforms into NO_2 in the atmosphere (Monks et al., 2015). In colder climates, such as Canada, residential heating can significantly raise NO_2 concentrations during the winter months (Government of Canada, 2023; Natural Resources Canada, 2022).

In addition to these, lightning and soil emissions from agricultural fields may contribute to NO_2 concentration as an important natural source (Leue et al., 2001; Schumann & Huntrieser, 2007). Although the contribution from lightning is smaller than anthropogenic sources, it may

play a role at regional scale NO_x concentration (Leue et al., 2001; Schumann & Huntrieser, 2007). Moreover, microbial processes in soils, particularly in agricultural fields where fertilizer is used, can become a prominent source of NO_2 concentration for agricultural regions (Granli & Bockman, 1994; Pilegaard, 2013).

O_3 does not emit directly to the atmosphere, instead, it forms through complex photochemical reactions with precursor pollutants, primarily NO_x and volatile organic compounds (VOCs) (Valacchi et al., 2004). The major precursor of O_3 formation is NO_2 which is emitted mostly from vehicular exhausts and industrial activities (Atkinson, 2000; Krivoshto et al., 2008; Sillman, 1999). Moreover, the use of solvents and consumer products such as paints, cleaning chemicals, etc. releases VOCs, and by reacting with NO_x and sunlight, it forms O_3 (Environmental Protection Agency, 2018). O_3 can be formed using natural sources precursors as well with biogenic VOCs like terpenes and isoprene released by natural vegetation playing a key role in the creation of O_3 in forested and rural areas (Guenther, 2007). Also, wildfire releases high amounts of NO_x and VOCs into the atmosphere, which has the potential for substantial O_3 formation when combined with sunlight over the impacted areas (Jaffe & Wigder, 2012; Johnson et al., 2010).

2.3 Behaviour of NO_2 and O_3 at the Atmosphere

Typically, nitric oxide (NO) is emitted from combustion processes and reacts with (O_3) in the atmosphere and forms NO_2 (Formula 1). During the daytime, the NO_2 undergoes photolysis in the presence of sunlight and produces NO and an oxygen atom (O) (Formula 2) (Seinfeld & Pandis, 2016). Subsequently, the free oxygen atom rapidly reacts with molecular oxygen (O_2) and forms O_3 (Formula 3) (Atkinson, 2000; Sillman, 1999). This confirms that O_3 concentration can be the highest during daytime (Sillman, 1999). NO_2 sometimes interacts with hydroxyl

radicals (OH) and forms nitric acid (HNO_3), which is known as a key element of acid rain (Formula 4) (Seinfeld & Pandis, 2016). This way NO_2 removal happens in the atmosphere.

$$NO + O_3 = NO_2 + O_2 \ldots\ldots\ldots\ldots (1)$$

$$NO_2 + Sunlight = NO + O \ldots\ldots\ldots\ldots (2)$$

$$O + O_2 = O_3 \ldots\ldots\ldots\ldots\ldots (3)$$

$$NO_2 + OH = HNO_3 \ldots\ldots\ldots\ldots\ldots\ldots (4)$$

Moreover, VOCs play a major role in to buildup of O_3 in the atmosphere, especially in high-emission areas from traffic and industrial activities (Amin et al., 2017; Atkinson, 2000). Initially, VOCs interact with OH and form peroxy radicals (RO_2) (Atkinson, 2000). Then the RO_2 react with NO and produce back to NO_2 without consuming O_3 (Sillman, 1999). This way O_3 increases in the atmosphere.

$$VOCs + OH = RO_2 \ldots\ldots\ldots (5)$$

$$RO_2 + NO = NO_2 + Products \ldots\ldots\ldots (6)$$

As O_3 is formed by interacting with NO_x and VOCs in the atmosphere in the presence of sunlight and other components, it can also be broken down through reaction with NO and other atmospheric substances (Formula 7) (Seinfeld & Pandis, 2016). This is known as O_3 titration (Seinfeld & Pandis, 2016). This process is significant near high NO emissions, for example, city centers, and can cause lover O_3 concentration in surrounding areas (Bolaji & Huan, 2013; Monks et al., 2015; Seinfeld & Pandis, 2016). On the other hand, in rural areas, less NO results in less titration and causes higher O_3 concentration.

$$O_3 + NO = NO_2 + O_2 \ldots\ldots\ldots\ldots (7)$$

At nighttime, the behavior of NO_2 and O_3 changes due to the absence of sunlight for photochemical reactions. So, NO_2 tends to increase, and O_3 generally decreases at night (Monks

et al., 2015). However, the titration process and interaction with other compounds and organic radicals may impact O_3 concentration in the atmosphere at nighttime.

2.4 Lifetime of NO_2 and O_3 at the Atmosphere

The lifetime of NO_2 and O_3 varies significantly based on factors like altitude, sunlight, environmental and meteorological conditions. NO_2 is a relatively short-lived pollutant compared to O_3 (Monks et al., 2015; Seinfeld & Pandis, 2016). The photolysis process of NO_x (Formula 2) notably reduces the lifetime of NO_2 (Seinfeld & Pandis, 2016). Thus, during the day, NO_2 may only last a few hours (Seinfeld & Pandis, 2016). Moreover, the NO_2 removal process (Formula 4) can further reduce this lifetime to a few hours during the day (Monks et al., 2015). At night, NO_2 lifetime expands to several hours to a day, as photolysis stops (Beirle et al., 2003).

The lifetime of O_3 is more complex than NO_2 because O_3 removal processes depend on altitude, environmental conditions, and meteorological conditions. Thus, O_3 lifetime varies from a few hours to weeks. During titration (Formula 7), O_3 shows a shortened lifetime of a few hours. However, during interaction with surfaces like vegetation, soil, and water, O_3 lifetime ranges from hours to a few days (Monks et al., 2015). This removal process is known as dry decomposition of O3 and is significant in rural and forest areas. In contrast, at higher altitudes (stratosphere) O_3 shows a much longer lifetime that varies from weeks to several months (Seinfeld & Pandis, 2016). Also, Stevenson et al. (2006) report O_3 lifetime on a global scale is approximately 22 days.

2.5 Recent Studies

Extensive research has been conducted globally to understand, analyze, and monitor air pollution. Also, the studies have covered a wide range of geographical areas, including urban, suburban, and rural regions, including Canada (Adams, 2020; Doiron et al., 2020; Griffin et al., 2020; S. R. Schneider et al., 2021), United States (Berman & Ebisu, 2020; Naeger & Murphy, 2020; Wu et al., 2020); Brazil (Bodah et al., 2022; Debone et al., 2020); Europe (Müller et al., 2022; P. Schneider et al., 2021); Asia (Huang & Sun, 2020; Shehzad et al., 2020); Middle East (Hashim et al., 2021; Shami et al., 2022); South Africa (Shikwambana et al., 2020); and worldwide (Bauwens et al., 2020; Cooper et al., 2022; Park et al., 2021). A few of the studies are detailed in table 2.1.

The studies have utilized various methods, including satellite remote sensing, ground-based monitoring, and modeling techniques, to analyze the distribution and patterns of air pollutants. For example, Griffin et al. (2020) utilized space-borne Sentinel-5P (TROPOMI) measured NO_2 dataset and the Global Environmental Multi-scale – Modelling Air Quality and Chemistry (GEM-MACH) model to study NO_2 emissions in Southern Ontario (Griffin et al., 2020). They found that NO_2 decreased by over 40% in Toronto and Mississauga, before and during the COVID-19 lockdown. They also presented their methodology for investigating other pollutants in different urban areas. Similarly, studies have been done by many other researchers around the globe, who employed a modeling approach to analyze air pollutants. For example, Lamsal et al. (2013) employed GEOS-Chem three-dimensional, Müller et al. (2022) utilized local indicator of spatial association (LISA), Shin et al. (2022) employed the Poisson regression model and Bayesian hierarchical model.

Table 2. 1. The details of some studies on air pollution from different parts of the globe

Authors	Study Area	Period	Pollutants studied	Data used
Adams, 2020	Canada	2015-2020	NO_2, NO_X, O_3, & $PM_{2.5}$	Google Community Mobility Report & Air quality station
Bauwens et al., 2020	Global scale	2019-2020	NO_2	Sentinel-5P (TROPOMI) & Ozone Monitoring Instrument (OMI)
Bodah et al., 2022	Brazil	2019-2020	NO_2 & CO	Sentinel-5P (TROPOMI) & Interview
M. J. Cooper et al., 2022	Global scale	2019-2020	NO_2	Sentinel-5P (TROPOMI)
Griffin et al., 2020	Canada	2019-2020	NO_2	Sentinel-5p (TROPOMI)
Hashim et al., 2021	Iraq	2020	NO_2, O_3, $PM_{2.5}$ & PM_{10}	Sentinel-5P (TROPOMI)
Huang & Sun, 2020	China	2005-2020	NO_2	Sentinel-5P (TROPOMI) & OMI
Lamsal et al., 2013	Global scale	2005-2007	NO_2	OMI
Müller et al., 2022	Germany	2018-2019	NO_2	Sentinel-5P (TROPOMI), Sentinel-2 (for LULC) & GEOSTAT 2011 V2.0.1 gridded population data
Naeger & Murphy, 2020	USA	2019-2020	NO_2 & $PM_{2.5}$	Sentinel-5P (TROPOMI), OMI, Air quality station, Vehicle-hours traveled (VHT) & Vehicle-miles traveled (VMT)
Park et al., 2021	Global scale	2018-2020	NO_2, CO_2 & CO	Sentinel-5P (TROPOMI) & Orbiting Carbon Observatory-2 (OCO-2)
S. R. Schneider et al., 2021	Canada	2001-2019	NO_2, $PM_{2.5}$, O_3, & CO	Air quality station
P. Schneider et al., 2021	Norway	2018-2020	NO_2	Sentinel-5P (TROPOMI)
Shehzad et al., 2020	India	2020	NO_2	Sentinel-5P (TROPOMI)
Shin et al., 2022	Canada	2001-2012	NO_2, $PM_{2.5}$ & O_3	Air quality station Meteorological station Canadian health information

A study by Naeger & Murphy, (2020) analyzed the impact of COVID-19 on NO_2 and $PM_{2.5}$ concentrations in four California cities (i.e., Los Angeles, Bakersfield, Fresno, and San Francisco) through in-situ measurements and space-borne datasets. They utilized OMI and TROPOMI datasets, California Air Resources Board (CARB) station measurements, vehicle-hours traveled (VHT) and vehicle-miles traveled (VMT) data. The findings indicated significant reductions in tropospheric NO_2 by 40% in Los Angeles, 38% in Fresno, and around 20% in Bakersfield and San Francisco in 2020, compared to 2019. Adams, (2020) utilized Google's COVID-19 Community Mobility Report and in-situ measurements and analyzed air pollution in Ontario during the COVID-19 state of emergency. He found a clear reduction in NO_2 and NO_x, a weaker reduction in O_3, and no decrease in $PM_{2.5}$. He suggested exploring the lasting effects of these changes on the health and mobility sector. Likewise, numerous studies utilized both satellite remote sensing data and station measurements and found significant changes in the air pollutants they considered (Bodah et al., 2022).

Interestingly, Müller et al. (2022) analyzed the spatial patterns of tropospheric NO_2 over Germany using the Sentinel-5P level-2 NO_2 dataset, Sentinel-2 LULC for 2016, and 1 km^2 gridded population data. They conducted hot and coldspot analyses and investigated the impact of meteorological factors on NO_2, finding that NO_2 hotspots were present in dense urban areas while coldspots were found in rural areas. Factors such as population road density, and impervious surface also had a strong impact on NO_2 variability. The study established that the spatial variability of NO_2 is influenced not only by local factors but also by the advection of surrounding geo-settings.

A comprehensive spatiotemporal assessment of selected air pollutants has not yet been conducted. Many researchers recommend studying the air pollution scenario for regular

monitoring (Adams, 2020; Griffin et al., 2020). More research is required to improve our understanding of the spatiotemporal dynamics of these pollutants in Canadian cities, particularly on a daily scale. Therefore, the present study has been undertaken to assess the temporal and spatial distribution of NO_2 and O_3 across Edmonton for five consecutive years (2018-2023). Subsequently, the relationship of the pollutants with elevation, temperature, road density, and population density has been investigated in the research work.

Chapter 3 Methodology

The methodology is described in four subsections. Firstly, the study area provides geographic and demographic details about Edmonton City. Secondly, data acquisition gives detailed information about the datasets used in the present study, the sources and characteristics of the datasets, and the data acquisition process. Also, the data collection steps using Google Earth Engine (GEE) are detailed in this section. Thirdly, the data processing section provides step-by-step procedures to process NO_2 and O_3, temperature, elevation, road network, and station-measured NO_2 and O_3 data. For example, data cleaning, outlier identification, formatting, and arranging datasets for analysis. Fourthly, the analysis section provides further details about the analysis carried out for the study and how that analysis has been performed to address the research questions. The analysis performed in the study are temporal and spatial analysis of satellite-derived NO_2 and O_3; and correlation assessment of explanatory variables with satellite-derived NO_2 and O_3.

3.1 Study Area

The present study focuses on Edmonton, Alberta's capital city between 53.5461° N and 113.4938° W (Lee, 2020) (Figure 3.1). The city is in the central region of the province along the North Saskatchewan River and is recognized as North America's northernmost large city (City of Edmonton, 2016). It covers 627.20 km^2 of land areas with a population of 1,151,635 and a population density of 1836.2 per km^2 in 2021 (Statistics Canada, 2022a). It is one of the fastest-growing cities in Canada, among the cities with over one million population with a population growth rate of 20% from 2011-2021 (Statistics Canada, 2022a). The city is expecting 2.2 million residents by 2044 (City of Edmonton, 2017). The mean elevation of the city is around 680m

however, it significantly varies surrounding the North Saskatchewan River valley between 600m to 700m (Figure 3.1) (City of Edmonton, 2023; Natural Resources Canada, 2023). The valley has a beautiful natural landscape with flat river terraces and steep slopes.

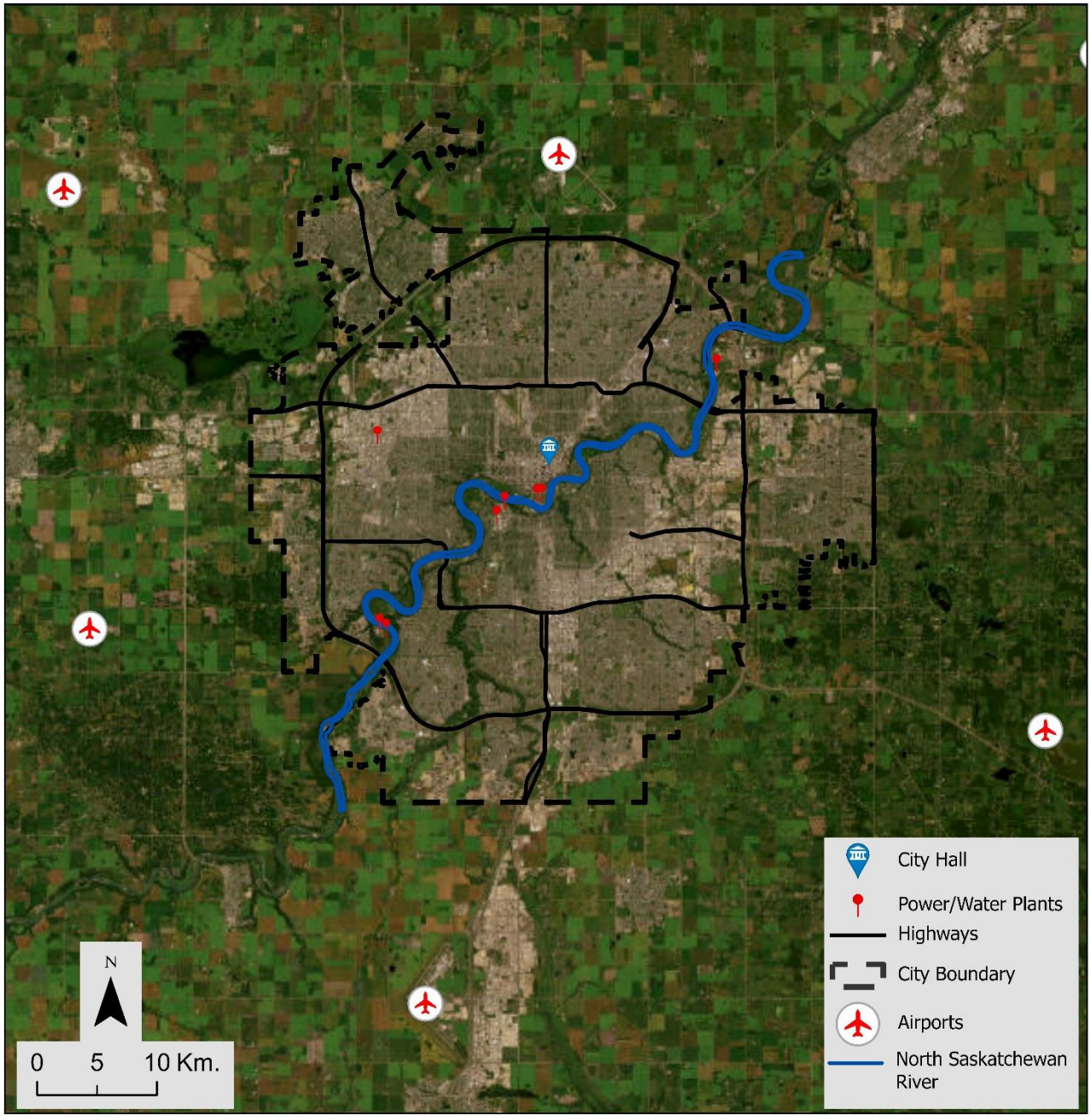

Figure 3. 1 Geographical settings of the study area

Edmonton has a humid continental climate and typically experiences extreme freezing, and dry winters (City of Edmonton, 2016; Muller, 2012; Powell, 1978). The city enjoys an abundance of sunshine throughout the year. The city experiences about 325 sunny days annually, with nearly 120 of those occurring during the winter months (City of Edmonton, 2016).

Edmonton's economy is diverse, with significant contributions from industries such as oil and gas, petrochemicals, and manufacturing (Government of Alberta, 2022a). The city hosts major industrial areas, particularly in the northern and southeastern parts, including the Edmonton Energy and Technology Park and the Nisku Industrial Park. These areas are hubs for heavy industries, including refineries and manufacturing plants, which contribute to the city’s economic growth but also pose challenges for air quality management (Government of Alberta, 2022a).

3.2 Data Acquisition

This study utilizes multi-sensor satellite remote sensing data, ground-based air pollution observations, high-resolution digital elevation model (HRDEM), road network, population data, and population center boundary to conduct the study (Table 3.1). Satellite retrieved datasets were collected from July 1st, 2018, to June 30th, 2023, and further organized into five consecutive years starting from July to next year June. Such as July 2018 to June 2019 describes the year 2018-19, likewise years 2019-20, 2020-21, 2021-22, and 2022-23 are named. The subsequent sections present a general description of each dataset, followed by the methods adopted to answer each research question.

Table 3. 1. Properties of datasets used in the present study

Data/Sensor/Satellite	**Source**	**Properties**	**Resolution** (Spatial/temporal)
Sentinel-5P TROPOMI	Google Earth Engine (GEE)/Copernicus Sentinel 5P	Level-3, NO_2 and O_3, NO2_column_number_density O3_column_number_density	1113.2 m Twice a Day
ERA-5	Google Earth Engine (GEE)/Copernicus Climate Data Store	Air temperature (at 2m)	1113.2 m Daily
HR-DEM	Canada Open Data Portal (https://open.canada.ca/)	Airborne LiDAR data	1 m
Road network	Statistics Canada https://www.statcan.gc.ca/	-	-
Study area boundary	Statistics Canada https://www.statcan.gc.ca/	Population centre & census tract	-
	Non-spatial data		
Census data 2021	CHASS (https://datacentre.chass.utoronto.ca/)	Population density	-

3.2.1 Sentinel-5P

The Sentinel 5 Precursor satellite, widely known as Sentinel-5P, is operated by the European Space Agency (ESA). It has on-boarded TROPOspheric Monitoring Instrument (TROPOMI) sensor that continuously collects data in seven spectral bandwidths, i.e., UV-1 (270-300nm), UV-2 (300 – 370nm), VIS (370 – 500nm), NIR-1 (685 – 710nm), NIR-2 (745 – 773nm), SWIR-1 (1590 – 1675nm) and SWIR-3 (2305 – 2385nm) (European Space Agency, 2023b). TROPOMI has a spectral resolution ranging from 5 – 15km, with the capability to reach up to 50 km at wavelengths below 300nm (H. Eskes et al., 2019; Wieczorek, 2023).

Sentinel-5P provides us with a wide range of air pollution data products i.e., ozone (O_3), carbon monoxide (CO), methane (CH_4), formaldehyde (HCHO), nitrogen dioxide (NO_2), sulfur dioxide (SO_2), Glyoxal (CHOCHO) and aerosol with daily global coverage (Table 3.2). Based on the satellite's orbital path, it collects data twice or three times daily with a spatial resolution of 5.5km by 3.5km (Griffin et al., 2020; Siddiqui et al., 2022).

The data products are freely available in three processing concentrations. Level-0 includes raw data, while Level-1 products offer geo-located top-of-atmosphere earth radiances for each spectral band (Morillas et al., 2024). The Differential Optical Absorption Spectroscopy (DOAS) algorithm generates most Level-2 products, retrieving tropospheric and stratospheric vertical column densities (VCDs), like other satellite missions (H. J. Eskes & Eichmann, 2018). Level 3 products are derived from Level-2 products using the harp-converter drive tool with bin-spatial operation, creating a $0.01 \times 0.01°$ resolution mosaic that forms an orthorectified raster layer (Google Earth Engine, 2024d; Morillas et al., 2024). Level 3 data products are filtered to remove pixels with quality assurance (QA) values less than 80% for AER_AI; 75% for the

tropospheric_NO2_column_number_density band of NO_2, 50% for all other datasets except for O_3 and SO_2 (Google Earth Engine, 2024d, 2024e). Furthermore, Geffen et al., 2019 and Spurr et al. 2021 describe the details of the retrieval process of NO_2 and O_3 (Spurr et al., 2021; Van Geffen et al., 2019). Additionally, the Sentinel-5P documents library is a potential source for more details about the other products of Sentinel-5P (European Space Agency, 2024). All these products are available in near real-time (NRT) and offline (OFFL) formats. The NRT products become accessible within three hours of sensing, while OFFL products offer higher data quality but require longer processing times (Google Earth Engine, 2024d). Recently, these datasets have been made available in the Google Earth Engine (GEE) platform at reduced spatial resolution (1113.2 m).

Table 3. 2. Sentinel-5P data product details (European Space Agency, 2023b).

Sentinel-5P products	**Parameter(s)**	**Primary sources**
O_3	Ozone (O_3) total column, tropospheric column, stratospheric vertical profile	Transportation, industry, primary pollutants (e.g., NO_2)
NO_2	Nitrogen dioxide (NO_2) total column, tropospheric column	Transportation, industry
SO_2	Sulfur dioxide (SO_2) total column, layer height (TBC)	Industry, Agriculture
HCHO	Formaldehyde (HCHO) total column	Pressed-wood products, gas stoves, wood-burning stoves, and kerosene heaters
CHOCHO	Glyoxal (CHOCHO) total column	Biomass combustion and biogenic processes
CH_4	Methane (CH4) total column	Oil and gas systems, livestock enteric fermentation, landfills
CO	Carbon monoxide (CO) total column	Transportation or machinery that burns fossil fuels
Aerosol	Aerosol UV absorption index, layer height, optical depth (TBC)	Urban/industrial emissions

The present study collects *NO2_column_number_density* and *O3_column_number_density* data at 1113.2 m spatial resolution from the GEE platform. However, the GEE does not provide much information about the downsampling techniques in the data description (Google Earth Engine, 2024d, 2024e). The NO2_column_number_density refers to the "Total vertical column of NO_2 (ratio of the slant column density of NO_2 and the total air mass factor)."; and O3_column_number_density refers to "Total atmospheric column of O_3 between the surface and the top of atmosphere" (Google Earth Engine, 2024d, 2024e). The unit of both pollutants is mole/m^2. Importantly, Sentinel-5P collects data between 6-8 pm of Edmonton local time.

3.2.2 ERA 5 Air Temperature

The present study collects European Centre for Medium-Range Weather Forecasts (ECMWF) Reanalysis v5 (ERA-5) air temperature (at 2m) data from the GEE platform (Google Earth Engine, 2024c). The ECMWF is an independent intergovernmental organization supported by 35 states (ECMWF, 2024). ERA-5 data products are freely available for the entire globe, spanning from 1950 to latest date (Araújo et al., 2022; Grzybowski et al., 2023; Hersbach et al., 2020). It offers a spatial resolution of 0.25° × 0.25° and high temporal resolution data on an hourly basis (Araújo et al., 2022; Google Earth Engine, 2024c). The hourly data are aggregated on a daily, monthly, and annual scale (Google Earth Engine, 2024c; Muñoz Sabater, 2019). ERA-5 air temperature has been widely utilized (Araújo et al., 2022; J. Liu et al., 2020; McNicholl et al., 2021; Siddiqui et al., 2022).

Air temperature data is available at 11132m spatial resolution in GEE (Google Earth Engine, 2024c). Temperatures are observed at 2 meters above the surface of land, sea, or inland waters and calculated by interpolating between the lowest model level and the Earth's surface, considering the prevailing atmospheric conditions (Google Earth Engine, 2024c; Muñoz Sabater,

2019). Hersbach et al. (2020) and Muñoz Sabater, (2019) describe further details about the data retrieval process. The data is measured on the Kelvin (K) scale.

3.2.3 High-Resolution Digital Elevation Model

The High-Resolution Digital Elevation Model (HRDEM) product is generated from airborne LiDAR data (primarily in the south and study area Edmonton falls under this part) and satellite images (in the north) (Natural Resources Canada, 2023). This product is part of the CanElevation Series, which was developed to support the National Elevation Data Strategy implemented by NRCan. The data are available at either 1m or 2m spatial resolution. The 1m resolution datasets cover an area of 10km X 10km, while the 2m resolution datasets cover an area of 20km X 20km (Natural Resources Canada, 2023). The present study utilizes the 1m spatial resolution elevation

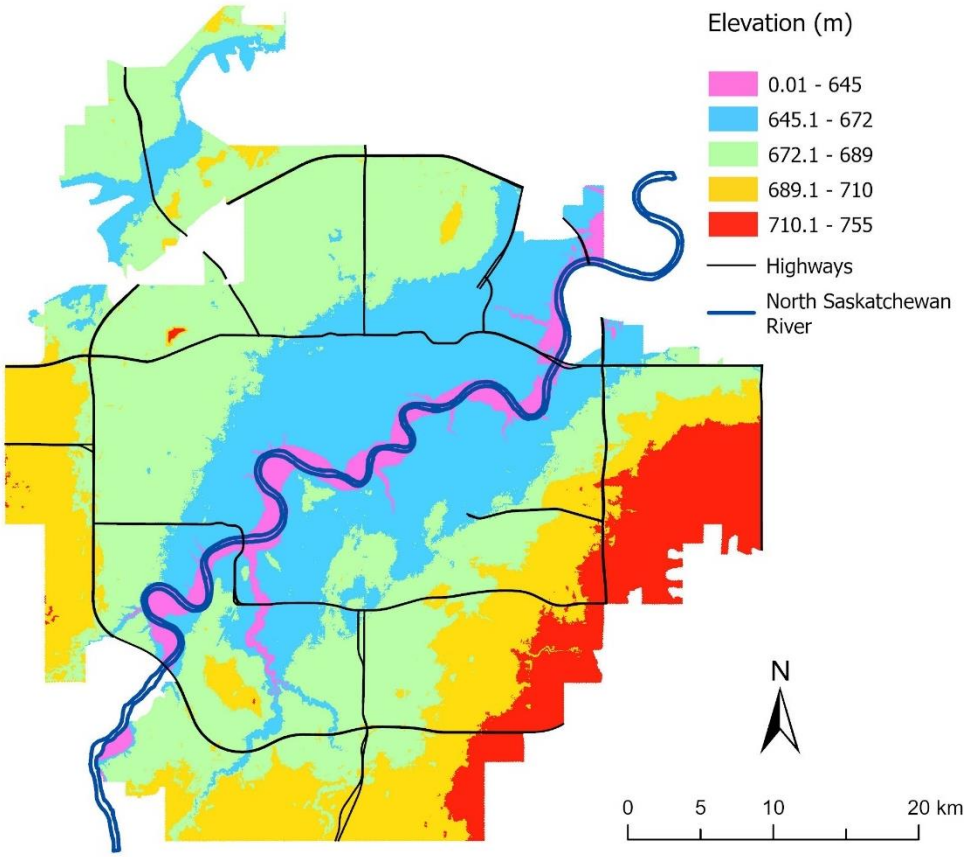

Figure 3. 2 Digital Elevation Model (referred to as elevation in the text) of the study area

(DEM). A total of 80 tiles are downloaded and mosaiced within ArcGIS Pro 3.1.2 (Figure 3.2). The final elevation (DEM) consists of 31526 columns and 35067 rows.

3.2.4 Road Network

The 2021 Census Road Network file was accessed from the Statistics Canada web portal in shapefile format (Statistics Canada, 2021). The data includes a unique identifier, DGUID, name, and type for each side of a street arc (where applicable) for provinces and territories, and census subdivisions. Streets are ranked according to five concentrations of detail: 1-Trans-Canada Highway, 2-National Highway System (not rank 1), 3-Major Highway (not rank 1 or 2), 4-Secondary Highway, Major Street (not rank 1, 2, or 3), and 5-All other streets.

3.2.5 Google Earth Engine (GEE)

The Google Earth Engine (GEE) is a web-based computing platform to conduct geospatial analysis, visualization, mapping, and downloading data (Google Earth Engine, 2024a; Jewell, 2023). It integrates a multi-petabyte collection of satellite imagery and geospatial datasets with planetary-scale analysis capabilities and enables Python and JavaScript in the code editor platform (Google Earth Engine, 2024a; Jewell, 2023; Kazemi Garajeh et al., 2023). The elements of the GEE environment are described in figure 3.3.

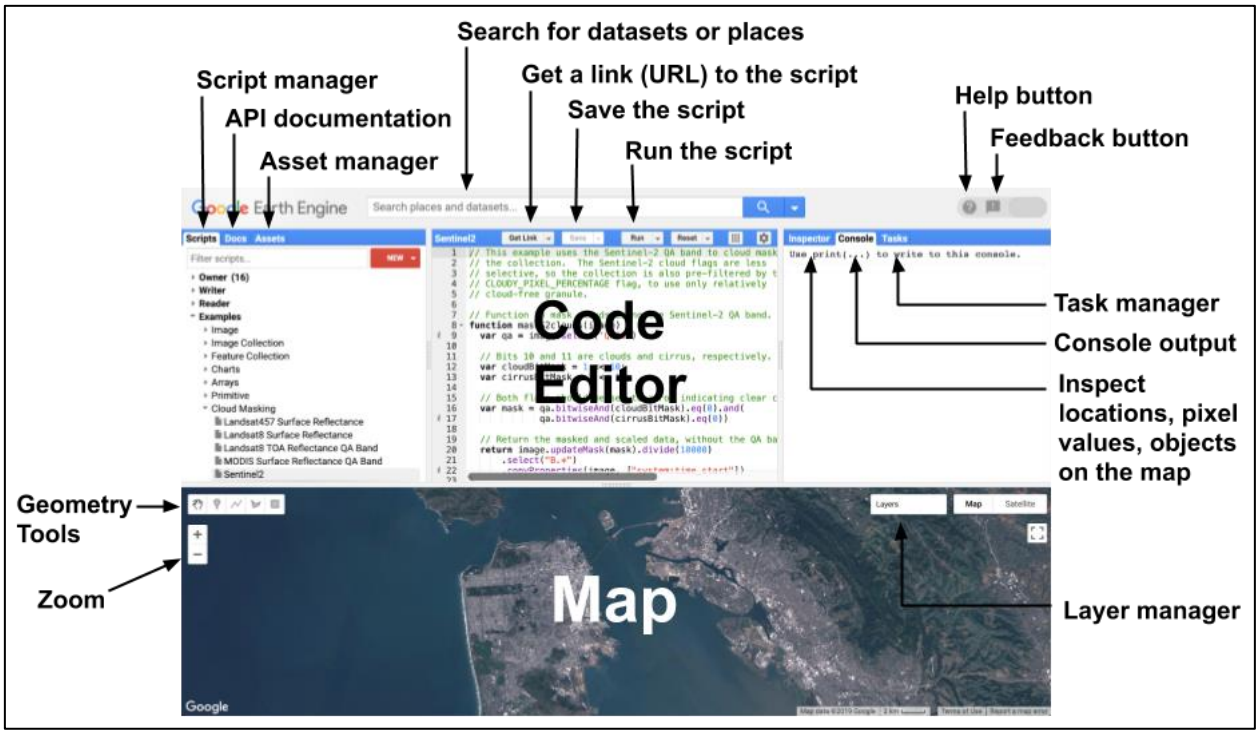

Figure 3. 3. Various components of GEE(Google Earth Engine, 2024b; Naeimi, 2021).

GEE has various kinds of object classes such as image collections, geometry, feature collection, reducer, etc. where, charts represent data like numbers, raster, strings, or vector (Google Earth Engine, 2024b; Naeimi, 2021). And each of the objects belongs to an individual class. Such as satellite images of different sensors are grouped together as a collection which is known as ImageCollection (Hossain, 2019; Naeimi, 2021). Each of the ImageCollection has a specific ID

and provides more details about the dataset under four tabs e.g., description, bands, image properties, and terms of use in the GEE data catalog (Google Earth Engine, 2024b). It is important to mention that the detailed function list is available under the 'Docs' tab in GEE (Figure 3.3, top left, API Documentation). Also, the 'Assets' tab (Figure 3.3, top left, Asset manager) enables to upload image (Acceptable formats are- GeoTIFF (.tif, .tiff) or TFRecord (.tfrecord + .json)), shape files (Acceptable formats are- .shp, .shx, .dbf, .prj, or .zip), and CSV files (Acceptable format .csv) (Google Earth Engine, 2024b). The present study uploads the study area Edmonton population center boundary (.shp) under 'Assets'. Initially, the study retrieves the datasets (as mentioned in Table 3.1) from the GEE platform and analyzes it in a desktop environment. The data retrieval steps from GEE are described below.

Steps to retrieve daily NO_2 and O_3 concentrations are as follows-

Step 1: The study imports image collections *"COPERNICUS/S5P/OFFL/L3_NO2"*, and *"COPERNICUS/S5P/OFFL/L3_O3"* separately in the GEE code editor. Also, imports the study area Edmonton population center boundary (.shp), which is previously uploaded and stored under the 'Assets' tab.

Step 2: The study filters the images by applying various filtering options in GEE.

Firstly, filters selecting specific bands (as mentioned in Table 3.1) *'NO2_column_number_density'* for NO_2, and *'O3_column_number_density'* for O_3.

Secondly, filters the images within the collection to include only those that intersect with the study area applying *'filterBounds'* as a spatial filter.

Thirdly, filters the images within the collection to include only those that fall within the date range from July 1st 2018 to June 30th 2023, applying *'.filterDate'* as a temporal filter.

Step 3: The study defines a function to process each image in the collection and convert it into a feature class as a CSV file for NO_2 and O_3. This function calculates the mean NO_2 and O_3 concentration for the image within the study area using the '*reduceRegion'* method, which applies a mean reducer *'ee.Reducer.mean()'* at a spatial resolution of 1113.2m (because the resolution of the selected bands is 1113.m). It also retrieves and formats the image's date. The mean concentrations and the formatted corresponding dates are then stored in a dictionary, which is set as properties of a new feature *'ee.Feature'*. The function returns this feature. Finally, the image collection is then mapped with the function and converts each image into a feature.

Step 4: Finally, the resultant feature collection from step 3 is exported to Google Drive as a CSV file. The export parameters are a description (Assign a name of the data product, such as NO_2/O_3), the folder on Google Drive (Assign a name of the folder, such as GEE), the file format as 'CSV', and the properties to be included in the export as the date and mean concentration.

Steps to retrieve annual mean NO_2, O_3, and temperature are as follows-

Step 1: The study imports three (3) image collections *"COPERNICUS/S5P/OFFL/L3_NO2"*, *"COPERNICUS/S5P/OFFL/L3_O3" and "ECMWF/ERA5_LAND/DAILY_AGGR"* separately and imports the study area boundary in the GEE code editor.

Step 2: The study filters selecting specific bands *'NO2_column_number_density'* for NO_2, *'O3_column_number_density'* for O_3, and *'temperature_2m'* for temperature. Filters the images

applying spatial filter *'filterBounds'*. Also, apply the temporal filter *'.filterDate'* for each year separately. Such as, the date ranges from July 1st 2018 to June 30th 2019 for the year 2018-19, likewise other subsequent years.

Step 3: To obtain a single representative annual mean image for NO_2, O_3, and temperature for five (5) consecutive years 2018-19 to 2022-23, the image collection is reduced by calculating the annual mean concentration of each band separately (using *'.mean()'*) across all images in the collection. Finally, it derives the annual mean image of NO_2, O_3, and temperature for the years 2018-19 to 2022-23 separately.

Step 4: The resultant annual mean images from step 3 are exported to Google Drive as a GeoTIFF file. The export parameters are a description (Assign a name of the data product, such as annual NO_2/O_3/Temperature), scale (refers to spatial resolution) as 1113.2m, region as study area boundary, the folder on Google Drive (Assign a name of the folder, such as GEE), the file format as 'GeoTIFF'.

3.3 Data Processing

3.3.1 Remote Sensing Data

Initially, the daily NO_2 and O_3 are collected for the study period (July 1st 2018 – June 30th 2023) from GEE in CSV format (.csv) (Described above under section 3.2.6). The study processes the CSV data on a desktop computer employing MS Excel. NO_2 has a total of 26,089 rows and O_3 has 24,885 rows. After removing the rows containing 'null' values and formatting the dates and values NO_2 remained 2,781 rows and O_3 3,074 during the study period. Therefore, the study calculates daily mean concentrations for NO_2 and O_3 during the study period.

Subsequently, the daily mean concentrations for NO_2 and O_3 are organized year-wise in separate Excel sheets. After organizing the data year-wise for both pollutants, the histogrsam of each year is analyzed and found extreme values. Afterward, extreme values are identified by using the Inter Quartile Range (IQR) method and removing them. IQR is a widely used statistical technique to identify outliers in a dataset (Barbato et al., 2011; Moore et al., 2009). It is a measure of statistical dispersion and is calculated as the difference between the first quartile (Q1- lower quartile value) and the third quartile (Q3- upper quartile value), and encompasses the middle 50% of the data (Barbato et al., 2011; Moore et al., 2009). The Formulas used to identify the extreme values are as follows-

$$IQR = Q3 - Q1 \quad (8)$$

Where Q1 is the first quartile (25th percentile) and Q3 is the third quartile (75th percentile).

$$Lower\ Limit\ (LL) = Q1 - 1.5 \times IQR \quad (9)$$

$$Upper\ Limit\ (UL)\ = Q3 + 1.5 \times IQR \quad (10)$$

$$Extreme\ Values\ =\ LL <\ or > UL \quad (11)$$

After removing the null values and outliers, overall, 90.1% of NO_2 data and 99.4% of O_3 data remains (Table 3.4). Data normality is checked visually by considering histograms, annual mean and median values, and skewness for both NO_2 and O_3.

Table 3. 3. Percentage of NO_2 and O_3 data used in the study

Pollutants	**2018-19**	**2019-20**	**2020-21**	**2021-22**	**2022-23**	**Overall**
			Percentage (%)			
NO_2	96.7	89.3	86.8	87.1	90.7	90.1
O_3	97.4	99.2	99.7	99.5	99.5	99.4

These datasets are used further to compute mean annual, monthly, seasonal, and weekdays for NO_2 and O_3 respectively. The four (4) seasons and months are Summer: June – August, Fall: September – November, Winter: December – February, and Spring: March – May. Subsequently, annual mean raster datasets of NO_2 and O_3 are imported and analyzed in ArcGIS Pro 3.1.2. The ERA-5 temperature data are converted into a degree Celsius (^oC) scale from Kelvin (K) using the raster calculator (C= K-273.16) (Figure 3.4).

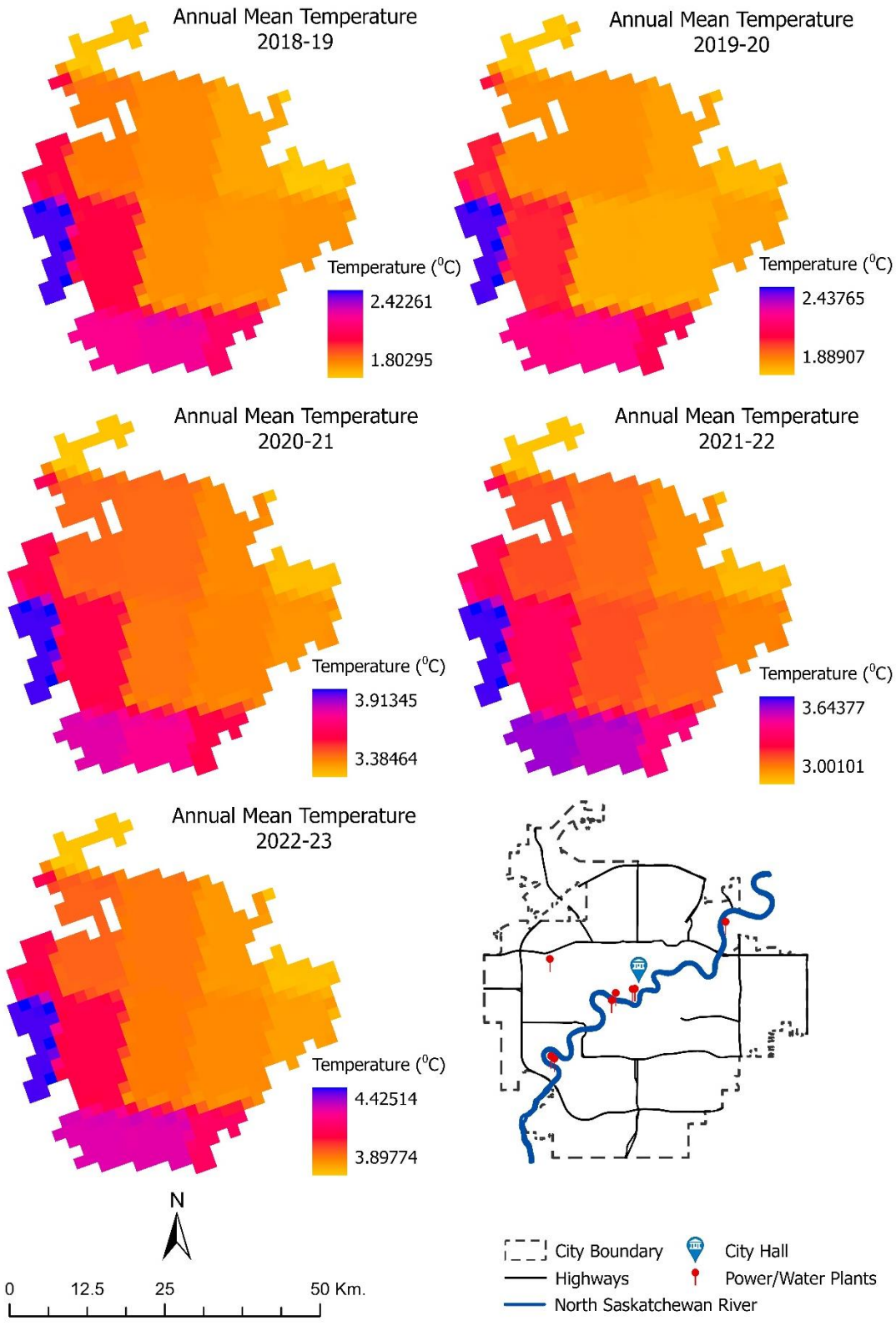

Figure 3. 4 Annual mean temperature of the study area

3.3.2 Road Density and Population Density

The road density is prepared using a line density tool, which utilizes all five (5) ranked roads (Figure 3.5). The default parameters are also kept unchanged (e.g., output cell size: 126m, search radius: 1051m, units: km^2). Initially, only major roads (rank 1-3 and rand 1-4) were considered to derive road density, however, the city's center and surrounding areas were giving very low road density, which seems like a wrong interpretation. Therefore, the study utilized all 5 types of roads.

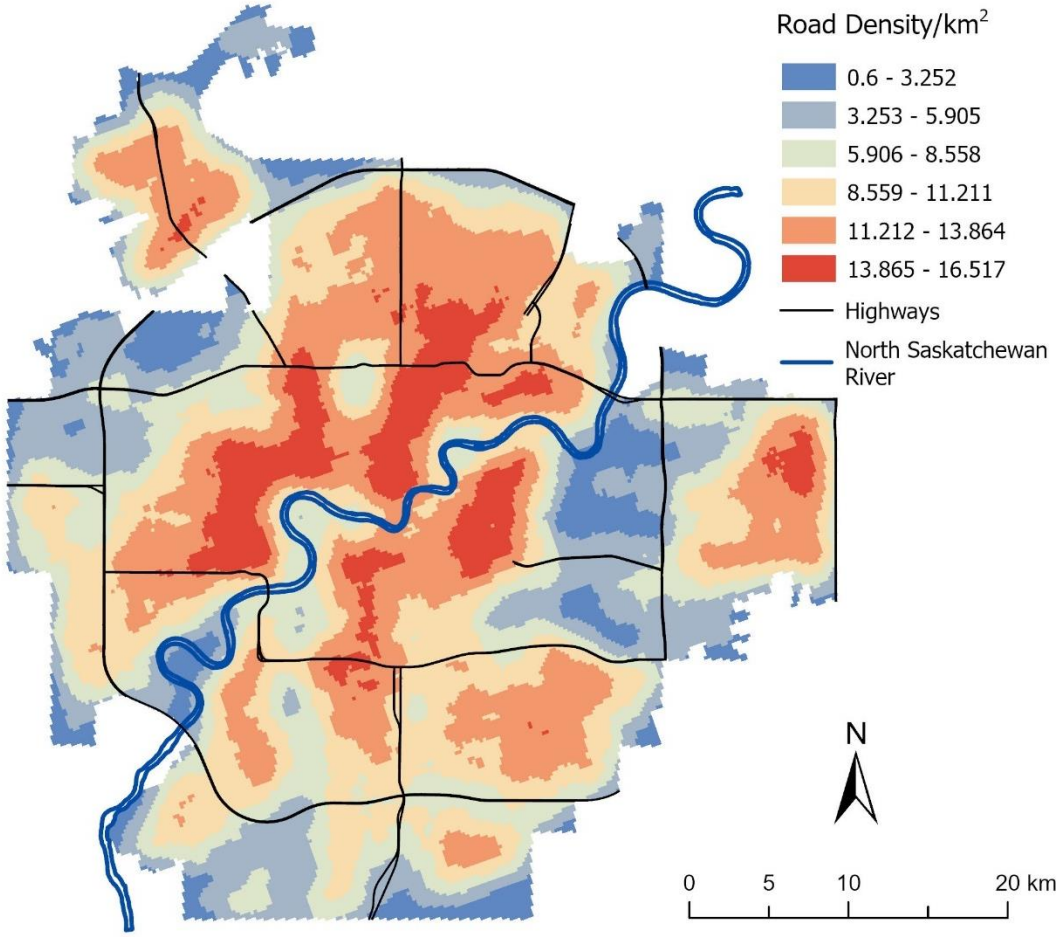

Figure 3. 5 Road density per km^2 utilizing all five classes of roads 1-Trans-Canada Highway, 2-National Highway System (not rank 1), 3-Major Highway (not rank 1 or 2), 4-Secondary Highway, Major Street (not rank 1, 2, or 3), and 5-All other streets (not rank 1, 2, 3, or 4)

Subsequently, the population density per km^2 for each of the Census Tracts is joined with census tract boundaries for Edmonton (Figure 3.6).

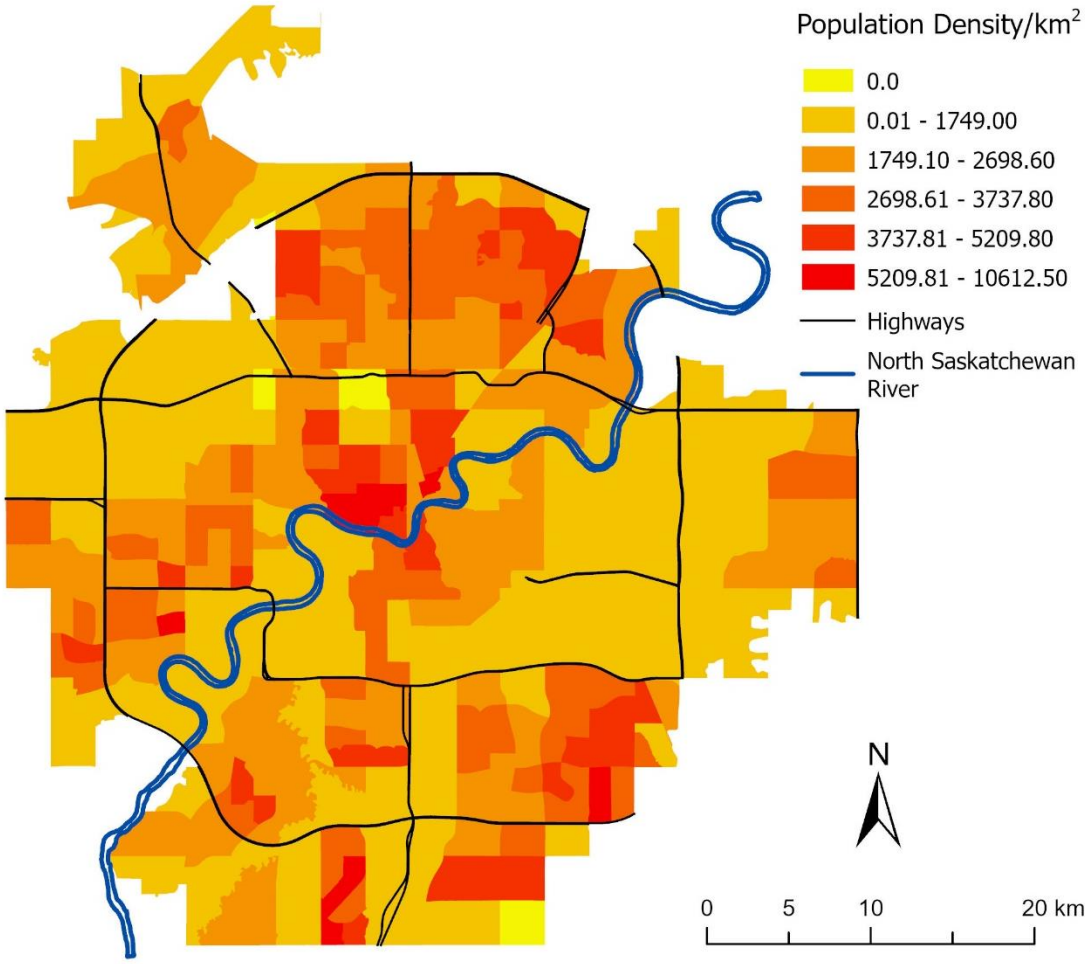

Figure 3. 6 Population density per km^2 of the study area shows 2021 population census data

3.4 Analysis

3.4.1 Temporal and Spatial Analysis of Sentinel-5P Retrieved NO_2 and O_3

The daily mean NO_2 and O_3 concentrations of Sentinel-5P are analyzed in four (4) temporal scales annual, seasonal, monthly, and weekdays during the study period (July 1st 2018 to June 30th 2023). The study utilizes MS Excel for temporal analysis. In the first place, daily mean NO_2 is selected for 2018-19 year, and the descriptive statistics are generated derived from 'Data Analysis' tools. Likewise, for the rest of the years, descriptive statistics are generated for NO_2. Similarly, descriptive statistics for O3 are also generated from the year 2018-19 to 2022-23. The daily mean NO_2 and O_3 concentration is further utilized and analyzed in the mean annual, seasonal, monthly, and weekdays fluctuations.

The distribution of NO_2 and O_3 concentrations during the COVID-19 period is also analyzed. Community transmission of COVID-19 has been confirmed in mid-March, followed by a state of emergency in all of the provinces of Canada (Adams, 2020; Tian et al., 2021). The study analyzes the daily mean of NO_2 and O_3 concentration and a 7-day moving average from February to May 2020 to understand the scenario.

Additionally, annual mean raster images of NO_2 and O_3 have been analyzed using ArcGIS Pro 3.1.2 to understand the spatial distribution of the pollutants in Edmonton City. The annual mean concentrations are classified using two different methods for better understanding the spatial distribution. Firstly, the annual mean NO_2 concentrations are classified into eight distinct categories using an equal interval method manually. Similarly, annual mean O_3 concentrations are classified into nine distinct categories. Secondly, the annual mean NO_2 and O_3 concentrations are classified into five classes using the Jenks Natural Breaks method (ESRI, 2024a).

Furthermore, these classes with higher value to lower value are renamed as very high, high, moderate, low, and very low accordingly. The study also performed hot spot analysis using the annual mean concentration images. To perform the hot spot analysis the study utilizes census tract boundaries of Edmonton City and the Optimized Hot Spot Analysis method (ESRI, 2024b). Therefore, thematic maps are prepared to incorporate key features (e.g., airports, highways, power plants, rivers, downtown) for a better understanding of the impacts of geo-settings on pollution scenarios.

3.4.2 Correlation of Explanatory Variables with Sentinel-5P Acquired NO_2 and O_3

The study compared the annual mean NO_2 and O_3 concentrations of Sentinel-5P with four explanatory variables elevation, annual mean temperature, road density, and population density of 2021. Firstly, the study converts the annual mean NO_2 and O_3 into point data (center point of the cell) for every year from 2018-19 to 2022-23. The points are used to extract annual mean temperatures, as the temperature data are in the same spatial resolution. Secondly, 1113m X 1113m polygons are created using a fishnet tool within the study area boundary and extracted mean values of elevation and road density for each of the polygons with the help of a zonal statistics tool. After that, the zonal statistics values are extracted under the points generated in the first step. Finally, these values are represented using scatter plots and drawn linear pattern lines along with R-square values. Additionally, a Person correlation is also assessed for understanding the relationship between pollutants and explanatory variables. The statistical significance test has been carried out with the p-value at 0.05. The relationship has been assessed individually to identify the strength and nature of each explanatory variables.

Chapter 4 Results

Temporal analysis was performed for annual, seasonal, monthly, and weekdays measurements of NO_2 and O_3 concentrations. The study performed hotspot analysis using satellite-derived yearly mean NO_2 and O_3 data. Furthermore, Pearson's correlation coefficient shows the relationship of pollutants with explanatory variables. Finally, the relationship between satellite-retrieved datasets and station-measured datasets was also assessed.

4.1 Temporal Analysis

Annual

The analysis across various temporal scales reveals distinct patterns influenced by anthropogenic activities and meteorological conditions. The annual mean NO_2 concentration shows a decrease in 2019-20 (94 µmol/m²) and an increase in 2022-23 (127 µmol/m²) (Table 4.1). In 2022-23, annual mean NO_2 concentration increases by approximately 21% compared to 2018-19. The annual median NO_2 concentration shows similar values across the study period except for a decrease in 2019-20 (Table 4.1). The annual mean standard deviation of NO_2 concentration shows a similar pattern during the first four years and increased by 86.7% in 2022-23 compared to 2018-19 (Table 4.1). The annual mean of minimum NO_2 concentration shows no pattern, where high and low values were observed in 2020-21 (23 µmol/m²) and 2022-23 (4 µmol/m²) respectively. Subsequently, the annual mean of maximum NO_2 concentration almost doubled in the year 2022-2023 (401 µmol/m²) compared to the year 2018-19 (211 µmol/m²). The annual mean of the 95^{th} percentile demonstrates similar values in the first four years and increased by more than 65% in 2022-23 (290 µmol/m²), compared to 2018-19 (175 µmol/m²). In all statistics,

2019-20 shows lower values, likely due to the restricted anthropogenic activities during the COVID-19 global pandemic.

Table 4. 1 Descriptive statistics of satellite-retrieved data for annual NO_2 and O_3, derived from daily mean data.

Statistics	2018-19	2019-20	2020-21	2021-22	2022-23	2018-2023
	NO_2 (µmol/m^2)					
Mean	104	94	105	107	127	107
Median	99	87	99	100	107	98
Standard Deviation (StD)	36	32	38	39	67	42
Minimum	16	17	23	14	4	15
Maximum	211	203	227	235	401	255
95th Percentile	175	160	183	189	290	199
	O_3 (mol/m^2)					
Mean	0.157	0.155	0.150	0.156	0.152	0.154
Median	0.157	0.153	0.149	0.155	0.150	0.153
Standard Deviation (StD)	0.019	0.020	0.021	0.019	0.022	0.020
Minimum	0.111	0.109	0.105	0.117	0.112	0.111
Maximum	0.206	0.201	0.205	0.216	0.209	0.207
95th Percentile	0.192	0.190	0.188	0.189	0.195	0.191

The annual mean O_3 concentration is relatively consistent, varying from 0.150 mol/m² in 2020-21 to 0.157 mol/m² in 2018-19 (Table 4.1). Median values are close to the mean, indicating a symmetric distribution of O_3 concentrations. The low fluctuation of standard deviation and 95th percentile reveals that O_3 concentrations are more consistent compared to NO_2 (Table 4.1). Lastly, the descriptive statistics highlight the divergent behaviours of NO_2 and O_3 pollutants, where NO_2 displays more dynamic changes likely influenced by human activities and environmental regulations, on the other hand, O_3 remains more consistent, possibly due to its formation and removal processes being more balanced.

The annual mean NO_2 shows a distinct increasing pattern, and O_3 does not show any pattern over the study period (Figure 3.1). Annual mean NO_2 decreases in 2019-20 and afterward increases over the period. However, the annual mean O_3 shows a decrease-increase-decrease pattern (Figure 4.1).

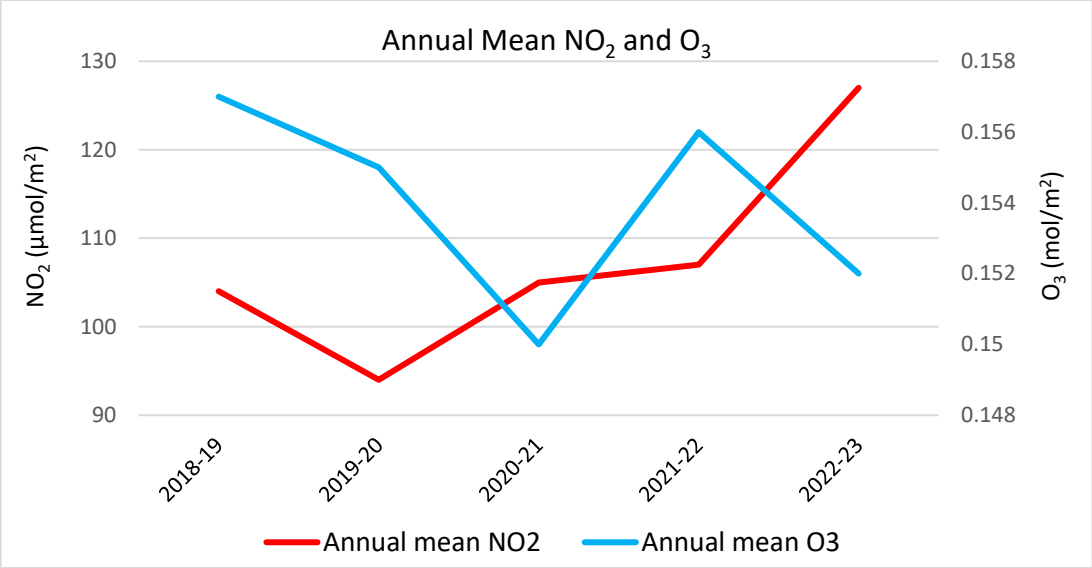

Figure 4. 1 Annual mean NO_2 and O_3 concentration

Seasonal

The seasonal mean NO_2 and O_3 concentration provides more insight into the patterns over the study period. During the summer seasonal mean NO_2 shows a relatively consistent pattern, with values ranging from 94 µmol/m² in 2019-20 to 107 µmol/m² in 2021-22 (Table 4.2). In fall, concentrations are consistently lower than in summer, and in spring vary widely, with a low of 88 µmol/m² in 2019-20 and a high of 140 µmol/m² in 2022-23 (Table 4.2). Seasonal mean NO_2 concentration peaks in the winter season, reaching its highest at 186 µmol/m² in 2022-23 (Table 4.2).

Overall, seasonal mean O_3 demonstrates a uniform pattern over the study period. Summer and fall mean O_3 concentrations are fairly consistent, varying from 0.141 mol/m² (2020-21) to 0.146 mol/m² (2021-22) and 0.132 mol/m² (2020-21) to 0.140 mol/m² (2021-22) respectively (Table 4.2). Winter and spring seasons show relatively higher concentrations over the study period compared to the other two seasons. The highest mean O_3 concentrations for the winter and spring seasons are 0.173 mol/m² (2019-20) and 0.177 mol/m² (2021-22) which are 4.2% and 5.1% higher than the overall seasonal mean of 2018-23 respectively.

In general, NO_2 shows the highest concentrations during winter, while O_3 peaks in winter and spring. The lowest NO_2 concentrations are observed in fall, whereas lower O_3 concentrations are noticed in fall and summer. In addition, NO_2 concentrations exhibit more variability across the seasons compared to O_3. Particularly, NO_2 has a significant spike in winter 2022-23, which is not observed in O_3 data. The increased concentrations during winter may be due to heating and excessive use of fossil fuel compared to the other seasons.

Table 4. 2 Satellite-retrieved seasonal mean NO_2 (µmol/m^2) and O_3 (mol/m^2), derived from daily mean data

Season	NO_2 (µmol/m^2)					
	2018-19	**2019-20**	**2020-21**	**2021-22**	**2022-23**	**2018-23**
Summer	103	94	100	107	102	101
Fall	100	90	94	101	99	97
Winter	113	111	116	115	186	128
Spring	103	88	117	110	140	112
	O_3 (mol/m^2)					
Summer	-	0.145	0.141	0.146	0.142	0.144
Fall	0.136	0.136	0.132	0.140	0.136	0.136
Winter	0.163	0.173	0.165	0.164	0.165	0.166
Spring	0.166	0.165	0.165	0.177	0.169	0.168

Monthly

The monthly NO_2 concentration peaks in February, with the highest recorded concentration of 222 µmol/m² in 2022-23 (Figure 3.2). February consistently shows higher values across the years, with an overall mean of 141 µmol/m². Subsequently, August has the lowest NO_2 concentrations, with a mean of 94 µmol/m² and the lowest value of 89 µmol/m² in 2019-20 (Figure 4.2). September and November also have relatively low means (95 µmol/m² and 96 µmol/m² respectively). Broadly, winter months (December, January, and February) show significantly higher NO_2 concentrations compared to other months (Figure 4.2). The summer

months (June, July, and August) have lower concentrations, with a slight increase in July. Furthermore, NO_2 shows notable annual variations, especially in the winter months. For instance, January and February of 2022-23 have considerably higher concentrations than previous years, demonstrating potential seasonal influences or specific annual events affecting NO_2 concentrations.

The highest monthly mean O_3 concentration is observed in February, with a mean of 0.176 mol/m² (Figure 4.3). March and April also show high O_3 concentrations, with means of 0.172 mol/m² and 0.174 mol/m² respectively. The lowest O_3 concentrations occur in September, with a mean of 0.131 mol/m². August and October also have relatively low means of 0.136 mol/m² and 0.134 mol/m² respectively. O_3 concentrations peak during the late winter and early spring months

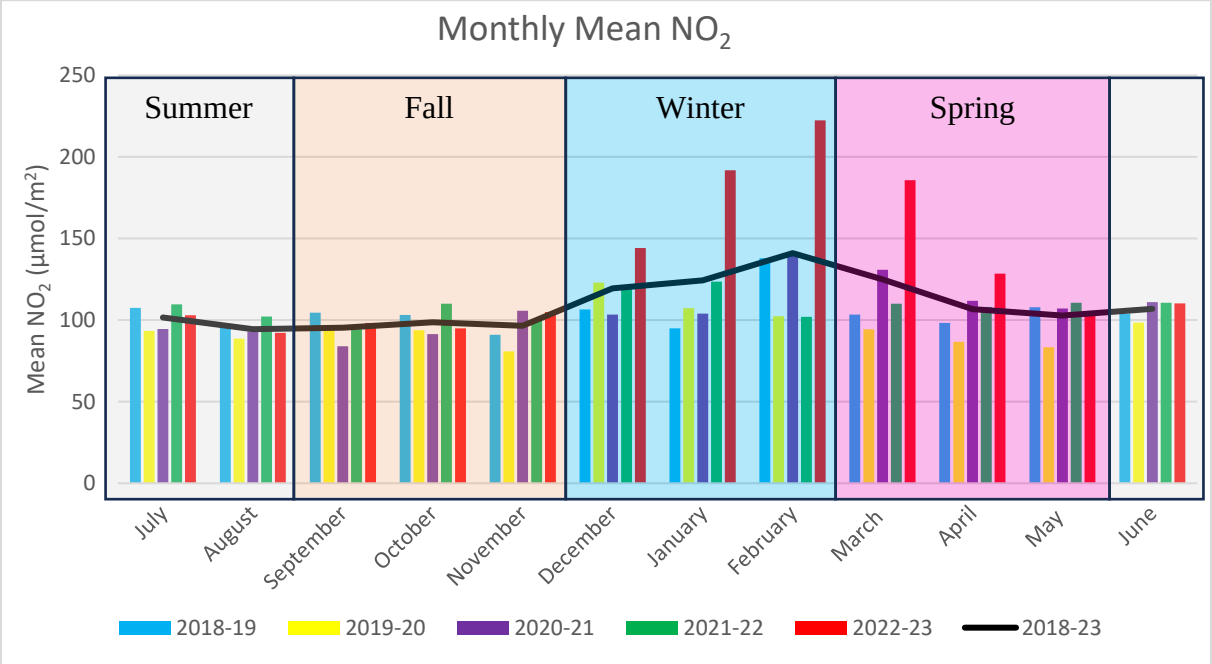

Figure 4. 2. Monthly mean of satellite retrieved data for NO_2 (µmol/m^2), derived from daily mean data

(February to April), and they are lower during the late summer and early fall months (August to October) (Figure 4.3). Subsequently, O_3 concentrations exhibit less variability than NO_2, maintaining more consistent concentrations across different years. However, there are slight

increases and decreases that align with seasonal changes. Interestingly, in 2022-23, O_3 concentrations mostly decreased whereas NO_2 shows the opposite.

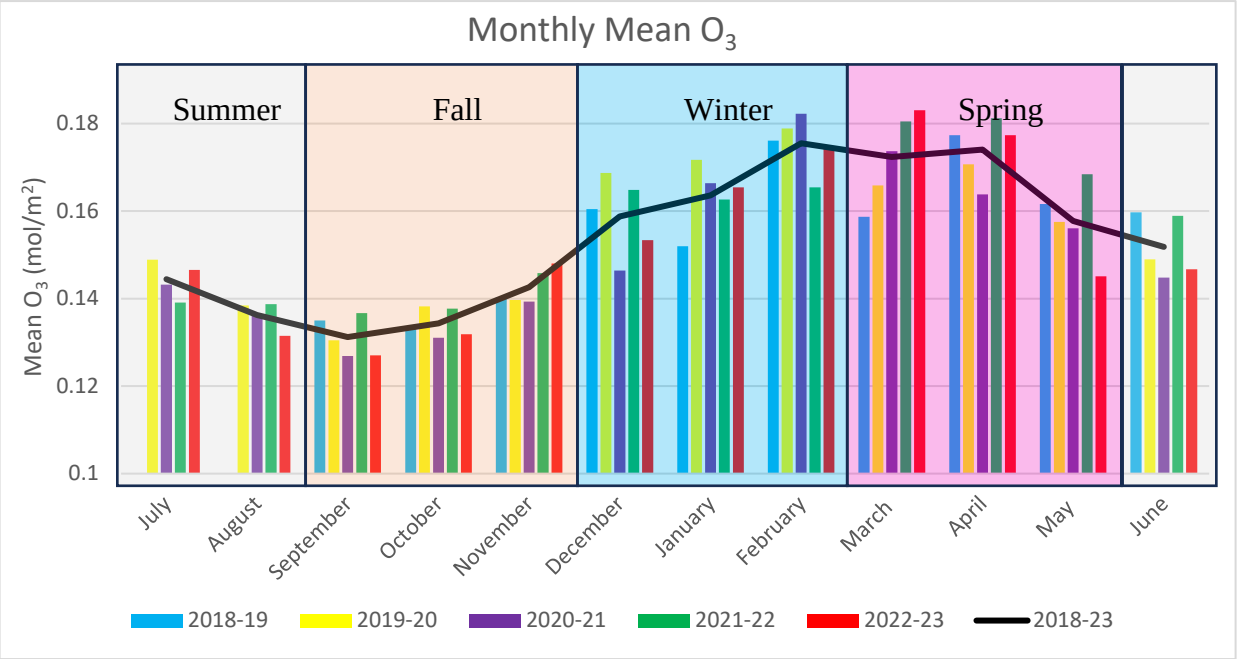

Figure 4. 3 Monthly mean of satellite retrieved data for O_3 (mol/m^2), derived from daily mean data

Weekdays

The weekdays mean distribution of NO_2 and O_3 concentration provides details about the air pollutants scenario during week days use and and weekends. The highest mean weekly days NO_2 concentration is observed on Wednesdays and Fridays (113 µmol/m²), with the highest single-day concentration on a Wednesday in 2022-23 (143 µmol/m²) (Table 4.3). Sundays consistently show the lowest weekdays mean NO_2 concentration (97 µmol/m²). Saturdays also exhibit a relatively low weekdays mean NO_2 concentration of 101 µmol/m² (Table 4.3). Notably, weekdays mean NO_2 concentrations are generally higher than on weekends. Moreover, throughout all days of the week, the year 2022-23 shows the highest weekdays mean NO_2 concentrations (Table 4.3). Weekdays mean O_3 concentration shows less fluctuations compared

to NO_2. Unlike NO_2, O_3 concentrations (weekdays mean) remain relatively consistent throughout the week, with no significant difference between weekdays and weekends.

Table 4. 3 Mean NO_2 and O_3 concentration on weekdays, derived from Sentinel-5P daily mean data

Days	NO_2 (µmol/m^2)					
	2018-19	**2019-20**	**2020-21**	**2021-22**	**2022-23**	**2018-23**
Monday	106	97	109	107	123	108
Tuesday	111	95	117	110	124	112
Wednesday	116	89	108	109	143	113
Thursday	112	95	103	113	118	108
Friday	100	97	114	114	141	113
Saturday	89	93	99	99	126	101
Sunday	99	92	85	99	109	**97**
	O_3 (mol/m^2)					
Monday	0.156	0.156	0.150	0.158	0.154	0.155
Tuesday	0.158	0.156	0.148	0.159	0.154	0.155
Wednesday	0.158	0.155	0.151	0.157	0.153	0.155
Thursday	0.153	0.153	0.150	0.157	0.152	0.153
Friday	0.156	0.152	0.150	0.154	0.152	0.153
Saturday	0.156	0.155	0.154	0.154	0.151	0.154
Sunday	0.159	0.155	0.15	0.156	0.151	0.154

COVID-19 Scenario

The daily mean NO_2 concentration decreased during the COVID-19 state of emergency (SOE) period from mid-March to the end of April 2020 compared to before SOE (Figure 4.4 A). The monthly mean NO_2 shows a similar pattern from February to May by 102, 94, 87, and 83 µmol/m² respectively (Figure 4.4 A). A 7-day moving average demonstrates smoother fluctuations over the period from February – May 2020 (post-SOE). In May 2020, NO_2 concentration decreased by 18.74% compared to February 2020 (pre-SOE). However, the daily mean O_3 concentration shows a different pattern with concentration declining in the early few days of SOE, followed by an increase from 10th April – 24th April 2020, and again declines afterward (Figure 4.4 B). The monthly mean O_3 concentration fluctuates from 0.179, 0.166,

0.171, and 0.158 mol/m² from February – May 2020, respectively (Figure 4.4 B). In May 2020, O_3 concentration decreased by 11.93% compared to February 2020 (pre-SOE).

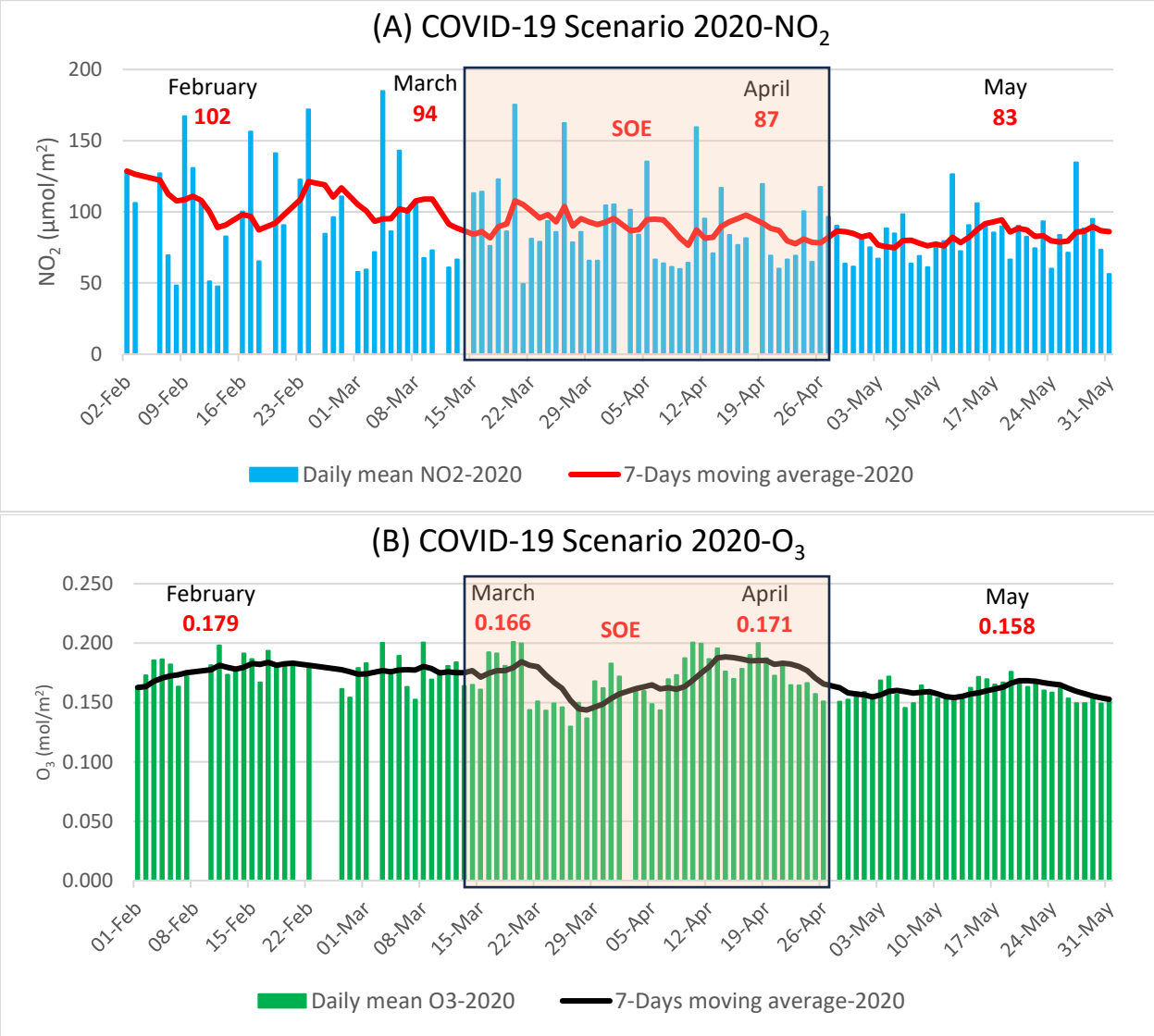

Figure 4. 4 Pre-during-post state of emergency (SOE) scenario 2020 for daily mean NO_2 (A) and O_3 (B) along with 7-day moving average

4.2 Spatial Analysis

4.2.1 Spatial distribution of Sentinel-5P retrieved annual mean NO_2 and O_3

NO_2 Distribution

The spatial distribution of annual mean NO_2 in Edmonton City from 2018-19 to 2022-23 shows distinct spatial and temporal variations (Figure 4.5). Across the study period, 2018-19 shows the highest annual mean NO_2 concentrations ranging between 120-157 µmol/m^2 and surrounds in central Edmonton, northeastern Edmonton, and southeast industrial areas (Figure 4.5). The following year (2019-20) shows the lowest annual mean NO_2 concentrations throughout the study area, between 81-120 µmol/m^2 (Figure 4.5). The subsequent years 2020-21 and 2021-22 show similar patterns, where annual mean NO_2 concentration ranges between low to moderate values. These two-years higher annual mean NO_2 concentration surrounds in northeastern Edmonton areas and lower annual mean NO_2 concentration surrounds southern, western, and north areas (Figure 4.5). Lastly, 2022-23 shows moderate to high annual mean NO_2 concentrations ranging from 110-156 µmol/m^2. In 2022-23, higher annual mean NO_2 concentration surrounds central Edmonton, northeastern Edmonton, and small parts of southeast Edmonton areas, and lower annual mean NO_2 concentration surrounds southwestern areas (Figure 4.5). In 2022-23, annual mean NO_2 concentration increases compared to the previous two years, however, the intensity of annual mean NO_2 concentration and area covered remains less than in the year 2018-19.

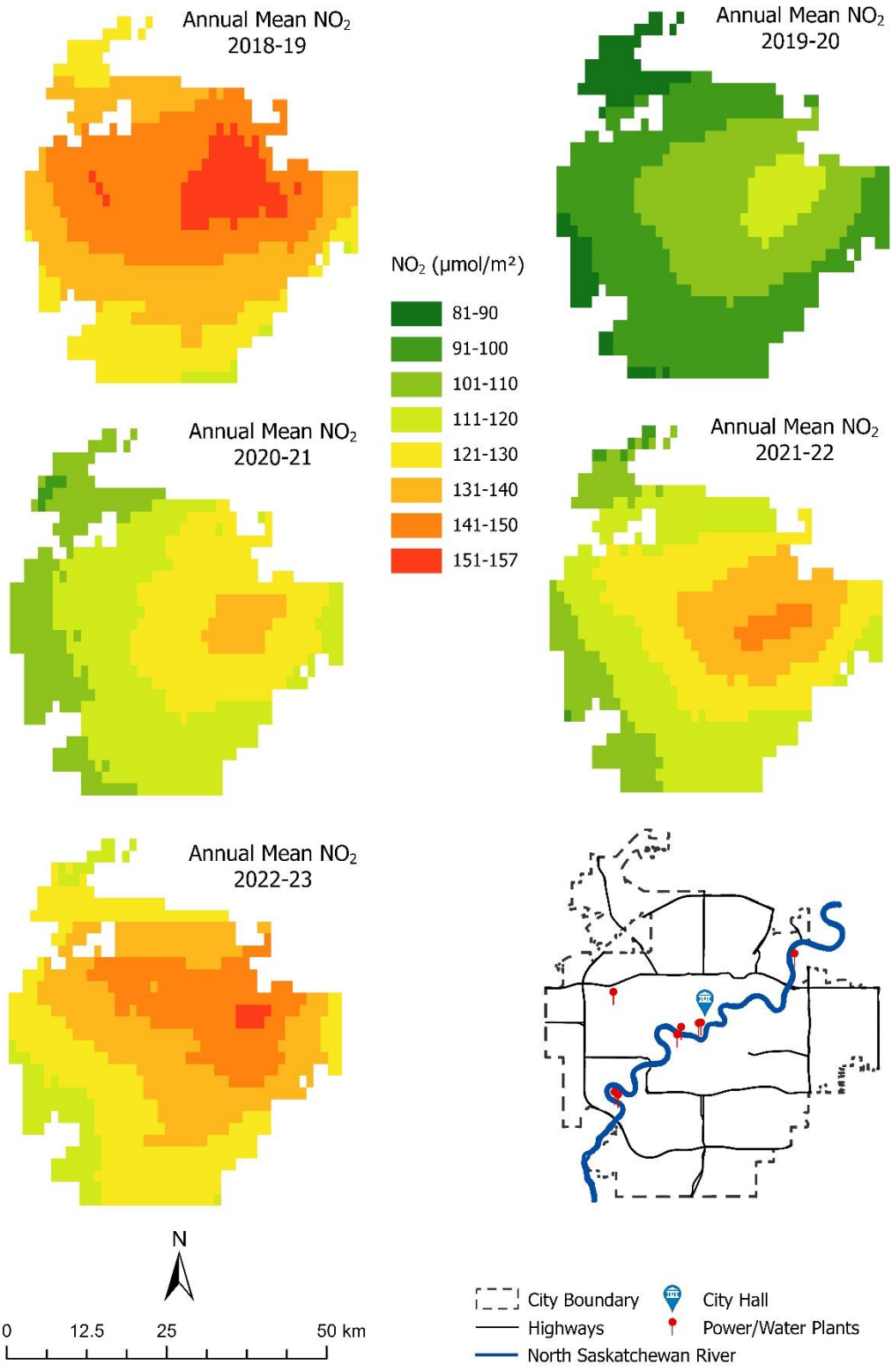

Figure 4. 5. Spatial distribution of annual mean NO_2 (Classes with equal interval method)

More detailed yearly patterns of annual mean NO_2 concentration are presented in figure 4.6. From 2018-19 to 2022-23 demonstrate similar spatial patterns of annual mean NO_2 concentration, however, the intensity varies over the period. Very high annual mean NO_2 concentration areas are found in downtown Edmonton, northeast Edmonton, and southeast industrial areas (Figure 4.6). In 2018-19, very high annual mean NO_2 covers an area of 141 km² (20% of total area) and gradually decreases to 85 km² (12% of total area) in 2022-23 (Table 4.4). High annual mean NO_2 concentration area covers 25% of the total area in 2018-19 and varies between 19-23% in the following years (Table 4.4). Moderate annual mean NO_2 shows a peak in 2019-20 by covering 29% of the total area and the rest of the year shows a consistent pattern and covers between 22-24% of the total area (Table 4.4). Low annual mean NO_2 concentrations cover 19% of the total area in 2018-19 and shows a peak in 2022-23 covering 28% of the total area (Table 4.4). Very low annual mean NO_2 concentration covers 13% of the total area in 2018-19 and reduced to 9% in the following year 2019-20, rest of years show a consistent pattern over the study period (Table 4.4).

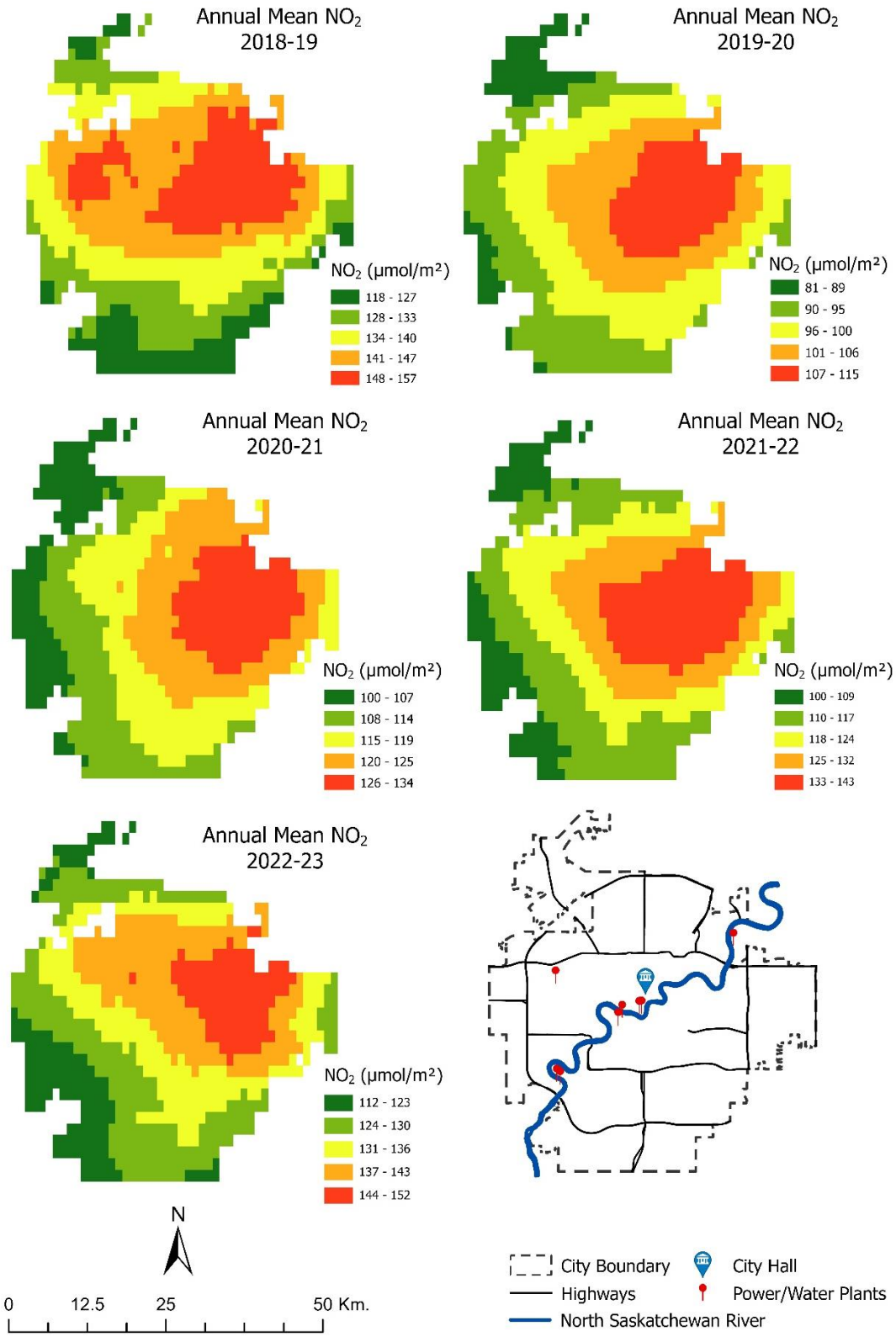

Figure 4. 6 Spatial distribution of annual mean NO_2 (Classes with natural break method)

Table 4. 4 Areal distribution of annual mean NO_2 and O_3

	2018-19			2019-20			2020-21			2021-22			2022-23		
		Area			Area			Area			Area			Area	
Class	Range	km^2	%	Range	km^2	%	Range	km^2	%	Range	km^2	%	Range	km^2	%
NO_2 (µmol/m^2)															
Very low	118-127	88	13	81-89	64	9	100-107	107	15	100-109	94	14	112-123	105	15
Low	128-133	132	19	90-95	168	24	108-114	146	21	110-117	190	27	124-130	191	28
Moderate	134-140	158	23	96-100	203	29	115-119	169	24	118-124	151	22	131-136	155	22
High	141-147	175	25	101-106	150	22	120-125	158	23	125-132	130	19	137-143	158	23
Very high	148-157	141	20	107-115	109	16	126-134	115	17	133-143	128	18	144-152	85	12
O_3 (mol/m^2)															
Very low	0.15809-0.15834	27	4	0.15482-0.15505	69	10	0.15061-0.15087	73	11	0.15679-0.15692	92	13	0.15212-0.15229	51	7
Low	0.15835-0.15850	134	19	0.15506-0.15516	172	25	0.15088-0.15097	107	15	0.15693-0.15705	84	12	0.15230-0.15239	123	18
Moderate	0.15851-0.15860	210	30	0.15517-0.15527	219	32	0.15098-0.15107	97	14	0.15706-0.15717	111	16	0.15240-0.15249	227	33
High	0.15861-0.15870	185	27	0.15528-0.15538	134	19	0.15108-0.15118	171	25	0.15718-0.15727	194	28	0.15250-0.15258	191	28
Very high	0.15871-0.15884	138	20	0.15539-0.15552	101	15	0.15119-0.15130	246	35	0.15728-0.15744	212	31	0.15259-0.15271	102	15

O_3 Distribution

The spatial distribution of annual mean O_3 concentration is heterogeneous from 2018-19 to 2022-23 (Figure 4.7). During the study period, 2018-19 shows the highest annual mean O_3 concentrations throughout the study area and ranges from 0.15701 to 0.15900 mol/m² (Figure 4.7). Next year 2019-20, annual mean O_3 concentration moderately decreases, ranging from 0.15401 to 0.15600 mol/m² (Figure 4.7). Subsequently, in 2020-21 Edmonton City experiences the lowest annual mean O_3 concentration across the study area, ranging from 0.15061 to 0.15200 mol/m² (Figure 4.7). In 2021-22, annual mean O_3 concentration increases followed by a decrease in 2022-23 and ranges from 0.15601 to 0.15800 and 0.15301 to 0.15400 mol/m² (Figure 4.7).

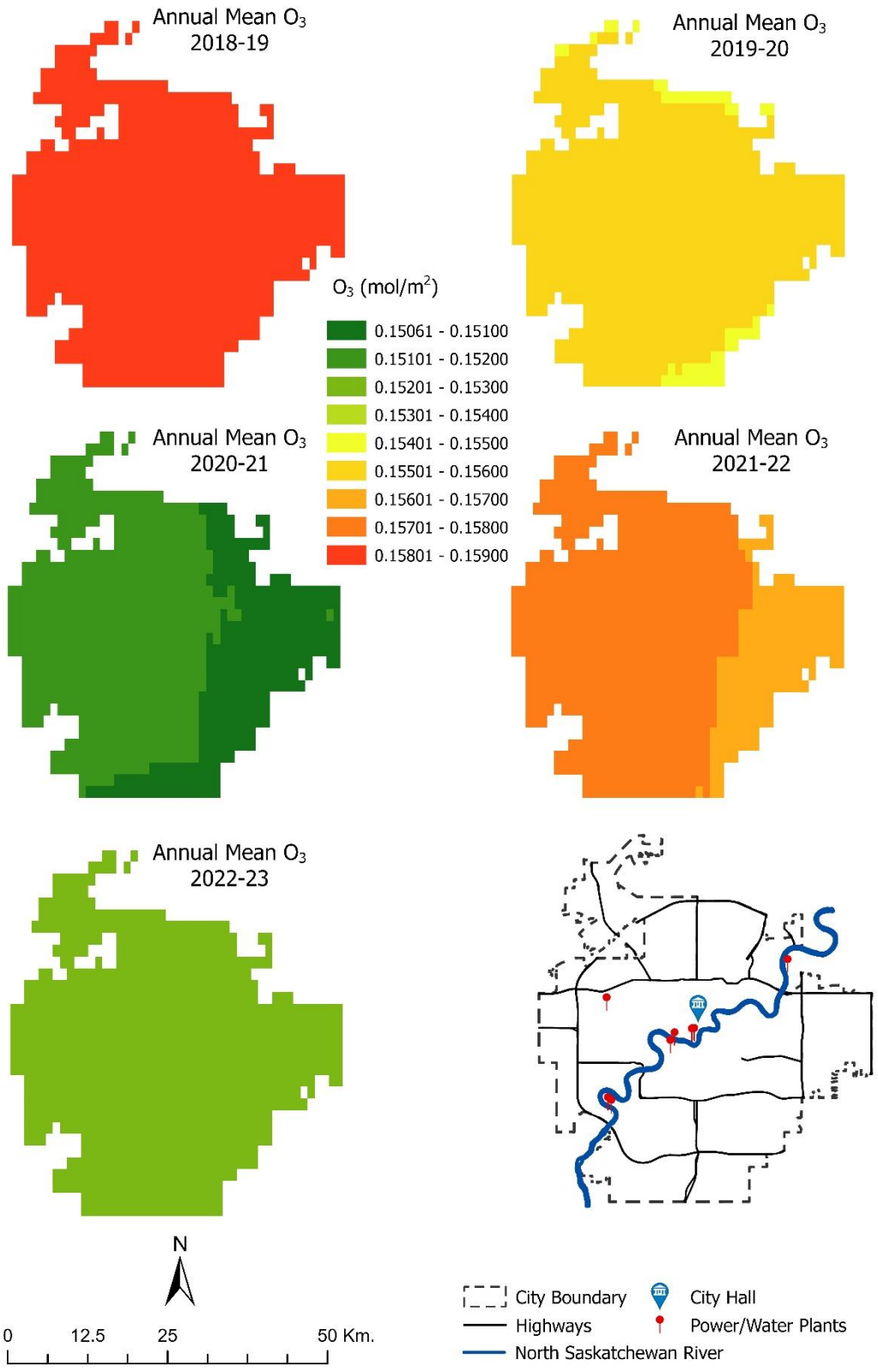

Figure 4. 7 Spatial distribution of annual mean O_3 (Classes with equal interval method)

The yearly patterns of annual mean O_3 concentration are more distinctly seen in figure 4.8. Individual years show a homogeneous distribution of annual mean O_3 concentration with varying intensities across the study period. Very high annual mean O_3 concentration area surrounds central, northern, and western regions (Figure 4.8). In 2018-19, very high annual mean O_3 concentration covers 20% of the total area followed by a decrease to 15% of the total area in both 2019-20 and 2022-23 and an increase to 35% and 31 % of the total area in 2020-21 and 2021-22 respectively (Table 4.4). High annual mean O_3 concentration covers 19% of the total area in 2019-20 and varies between 25-28% in other years (Table 4.4). Moderate annual mean O_3 concentration varies between 30-33% of the total area in years 2018-19, 2019-20, and 2022-23, and covers significantly less areas (between 14-16% of the total area) in 2020-21 and 2021-22 (Table 4.4). Low and very low annual mean O_3 concentration together covers 35% of the total area in 2019-20 and varies between 23-26% of the total area in other years (Table 4.4).

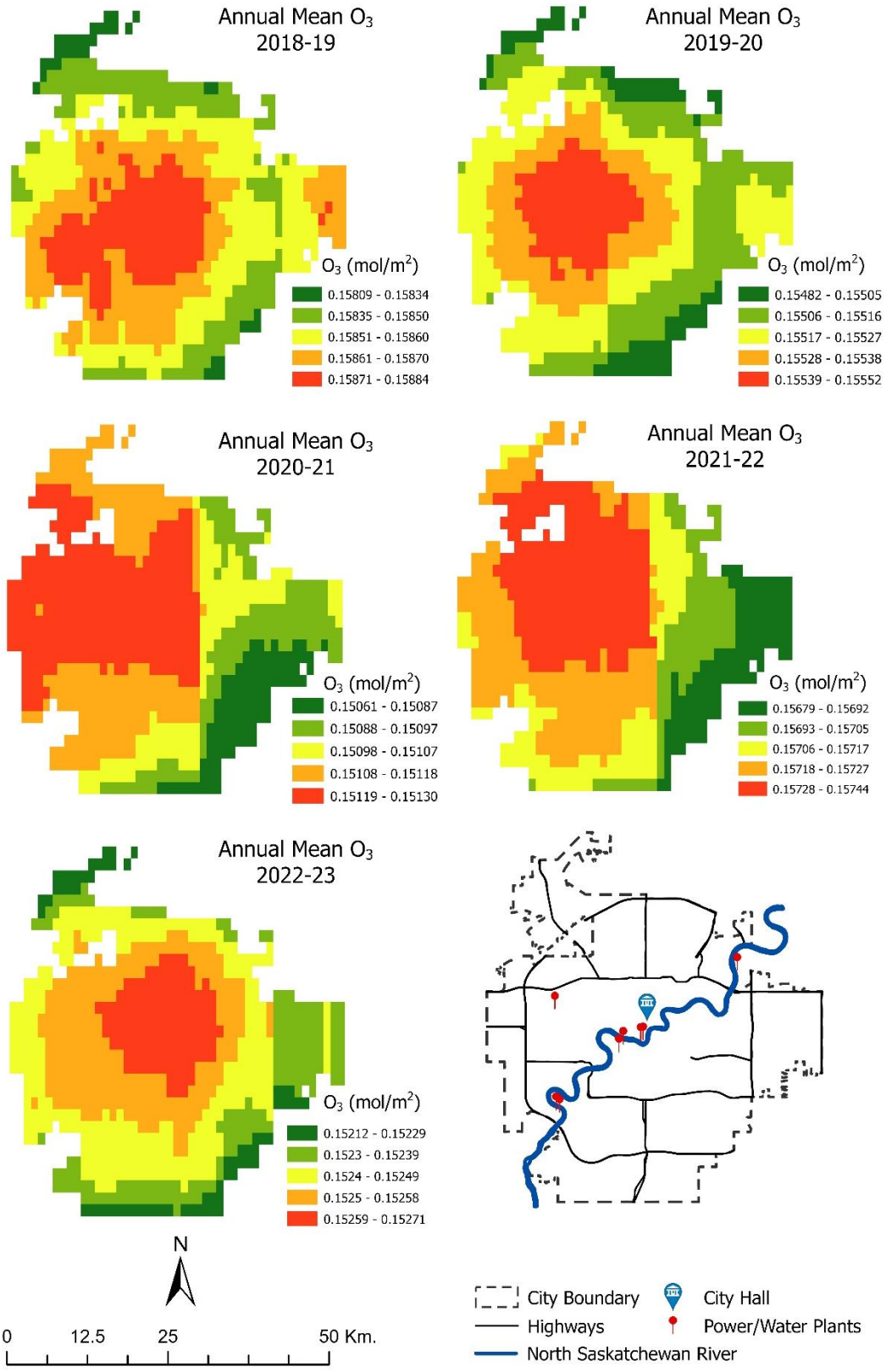

Figure 4. 8 Spatial distribution of annual mean O_3 (Classes with natural break method)

4.2.2 Hotspot analysis of Sentinel-5P retrieved annual mean NO_2 and O_3

Hotspot Analysis of NO_2

The hotspot analysis of annual mean NO_2 concentration shows the statistically significant areas of the highest and least NO_2 concentration with 90%, 95%, and 99% confidence level (Figure 4.9). The hot spots with a 99% confidence level cover small areas in central Edmonton and northeastern parts of Edmonton city in 2018-19, 2020-21, and 2022-23 compared to 2019-20 and 2021-22 (Figure 4.9). In 2019-20 and 2021-22, hot spots with a 99% confidence level cover large parts of central Edmonton and eastern parts of Edmonton City (Figure 4.9). While cold spots with a 99% confidence level shift over the study period. In 2018-19, cold spots with a 99% confidence level surround in a small area of outer northern Edmonton and large areas in the southern suburban region (Figure 4.9). In subsequent years, cold spots with a 99% confidence level expand westward and surround the outer peripheral regions of north, south, and west parts of Edmonton city (Figure 4.9). Overall, the hotspot analysis signifies that higher NO_2 concentration areas are consistent and concentrated surrounding central urban areas, and lower NO_2 concentration areas surround the suburban regions. The cold spot shifts slightly across the study period, but always in the outskirts of the city.

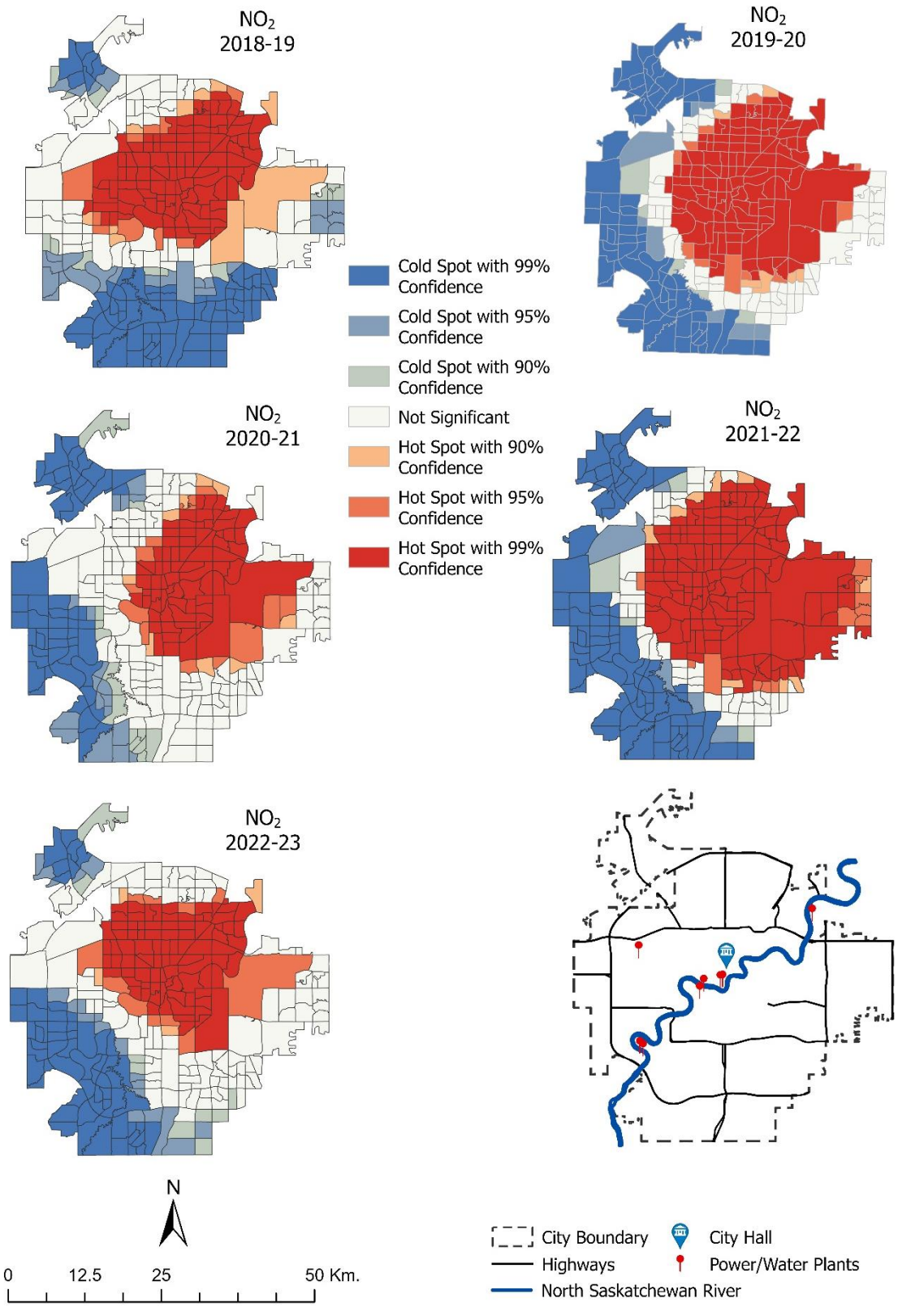

Figure 4. 9 Hot spot analysis of annual mean NO_2 using Optimized Hot Spot Analysis method

Hotspot Analysis of O_3

The hotspot analysis of annual mean O_3 concentration shows different patterns distinct from those of NO_2 (Figure 4.10). Overall, hot spots are more concentrated in the east and the central area, while cold spots are located on the outskirts, forming a north-west-south fringe. 2018-19 and 2019-20 show similar patterns for both hot and cold spots, where hot spots with 99% confidence level surround a large part of central Edmonton and western Edmonton, and cold spots with 99% confidence level are found in the outer north, northeast, and southeastern suburban areas (Figure 4.10). In the subsequent years, 2020-21 and 2021-22, hot spots with 99% confidence level slightly reduced in area, however, remain concentrated in the central Edmonton areas. Cold spots with a 99% confidence level surround the eastern and southeastern suburban peripheries in 2020-21 and 2021-22 (Figure 4.10). In 2022-23, hot spots with a 99% confidence level expand northward and remain concentrated in central Edmonton (Figure 4.10). Cold spots with a 99% confidence level cover southern and southeastern Edmonton with slight shifts in a small part of north Edmonton (Figure 4.10).

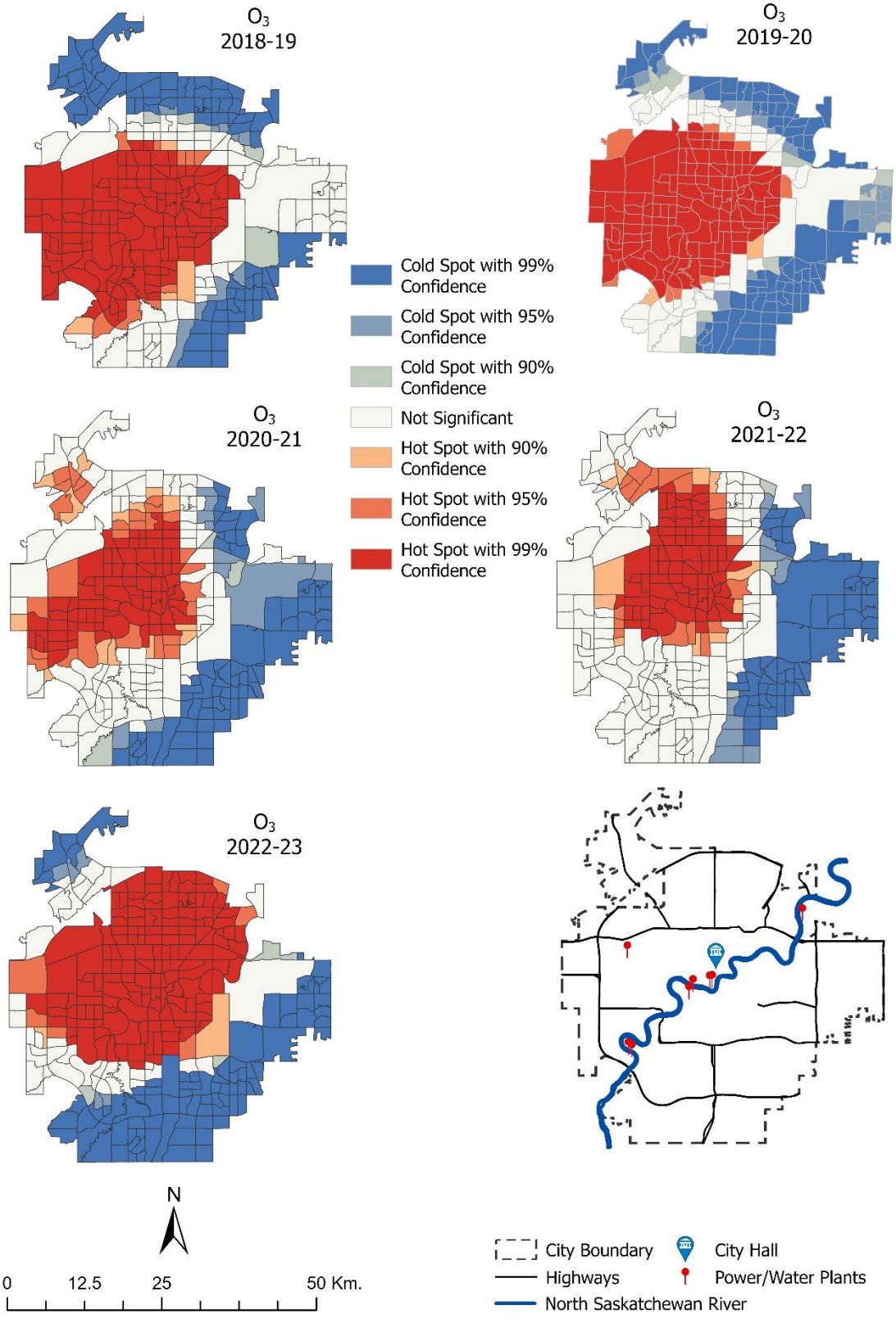

Figure 4. 10 Hot spot analysis of annual mean O_3 using Optimized Hot Spot Analysis method

4.3 Relationship of NO_2 and O_3 with Explanatory Variables

a. Elevation in relation to NO_2 and O_3

NO_2 shows a varying inverse relationship with elevation (Table 4.5 and Figure 4.11). In 2018-19, shows a moderately strong negative correlation (Pearson's correlation -0.57) between NO_2 concentration and elevation. Also, the coefficient of determination ($R^2 = 0.3287$) suggests that elevation explains a considerable amount of the variability in NO_2 concentrations during 2018-19. However, in 2019-20, the correlation weakens (Pearson's correlation -0.37) and, in the subsequent year, continues to decline further (Table 4.5). Similarly, R^2 values follow a decreasing pattern from 2019-20 to 2022-23 (Figure 4.11). The declining pattern of R^2 values suggests that elevation has little predictive power over NO_2 concentration. Overall, across the five years, Pearson's correlation is -0.39, which indicates a moderate association in the relationship between elevation and NO_2 concentration. The scatter plots suggest that higher elevation corresponds to lower NO_2 concentration (Table 4.5 and Figure 4.11).

Table 4. 5 Pearson's correlation of the satellite-measured NO_2 and O_3 concentration with elevation, air temperature, population density, and road density.

	Annual mean NO_2					
	2018-19	**2019-20**	**2020-21**	**2021-22**	**2022-23**	**2018-23**
Elevation	-0.57*	-0.37*	-0.22*	-0.31*	-0.30*	-0.39*
Temperature	-0.40*	-0.40*	-0.45*	-0.48*	-0.51*	-0.59*
Road Density	0.26*	0.26*	0.20	0.21	0.19	0.24*
Population Density	-	-	0.08	0.03	-	0.05
	Annual mean O_3					
	2018-19	**2019-20**	**2020-21**	**2021-22**	**2022-23**	**2018-23**
Elevation	-0.36*	-0.47*	-0.52*	-0.53*	-0.59*	-0.57*
Temperature	0.07	-0.06	0.17*	0.14*	-0.16*	0.05
Road Density	0.41*	0.39*	0.27*	0.33*	0.50*	0.43*
Population Density	-	-	-0.11	-0.05	-	-0.08

**All the value indicates statistically significant correlations at the 95% confidence level (p-value<0.05)*

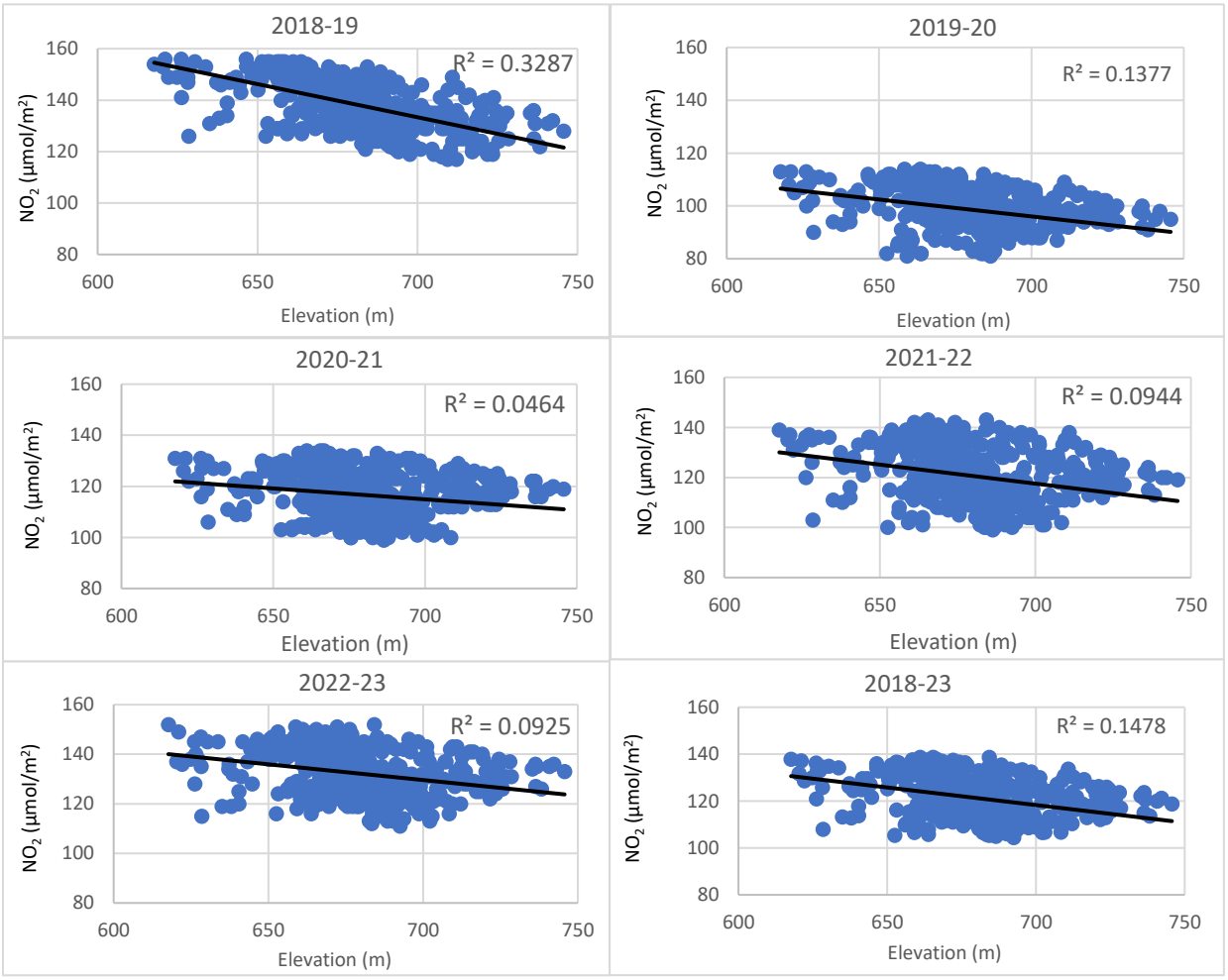

Figure 4. 11 The relationship between the satellite retrieved annual mean NO_2 and elevation

Pearson's correlation (Table 4.5) and the scatter plots (Figure 4.12) show a gradually increasing negative relationship between O_3 concentration and elevation over the study period. In 2018-19, O_3 shows a week inverse correlation with elevation (Pearson's correlation -0.36), followed by a gradual increase in subsequent years. In 2022-23, the correlation between O_3 concentration and elevation reaches its strongest point at −0.59 (Pearson's correlation). The scatter plots show some spread with an increasing pattern of R^2 values throughout the study period (Figure 4.12). The lowest R^2 value founds in 2018-19 (R^2 = 0.1287) and the highest in 2022-23 (R^2 = 0.3531) (Figure 4.12). Overall, during the study period, Pearson's correlation shows a moderate to strong inverse relationship between O_3 concentrations and elevation.

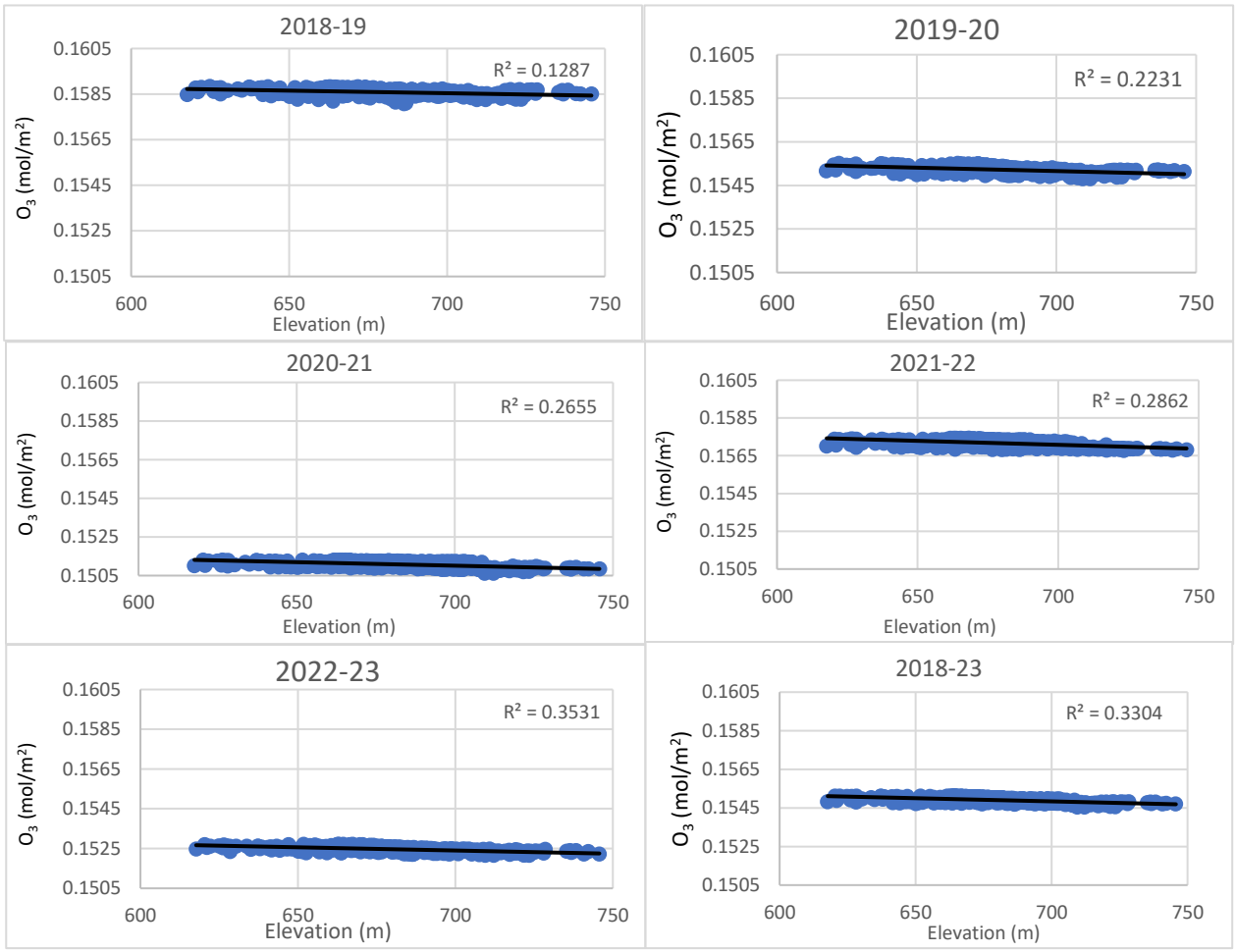

Figure 4. 12 The relationship between the satellite retrieved annual mean O_3 and elevation

b. Temperature in relation to NO_2 and O_3

Across the study period, NO_2 concentration and temperature show a consistent and strengthening negative correlation (Table 4.5 and Figure 4.13). In 2018-19, a moderate inverse relationship was found between NO_2 concentrations and temperature (Pearson's correlation -0.40). Following years, Pearson's correlation increases and becomes -0.51 in 2022-23 (Table 4.5). The scatter plots show an increasing pattern of R^2 values during the study period except 2019-20 (Figure 4.13). The patterns of R^2 values suggest that temperature explains about 23% to over 40% of the variability in NO_2 concentrations across the period. The relationship also suggests that temperature plays an important role in influencing NO_2 concentration in the study area.

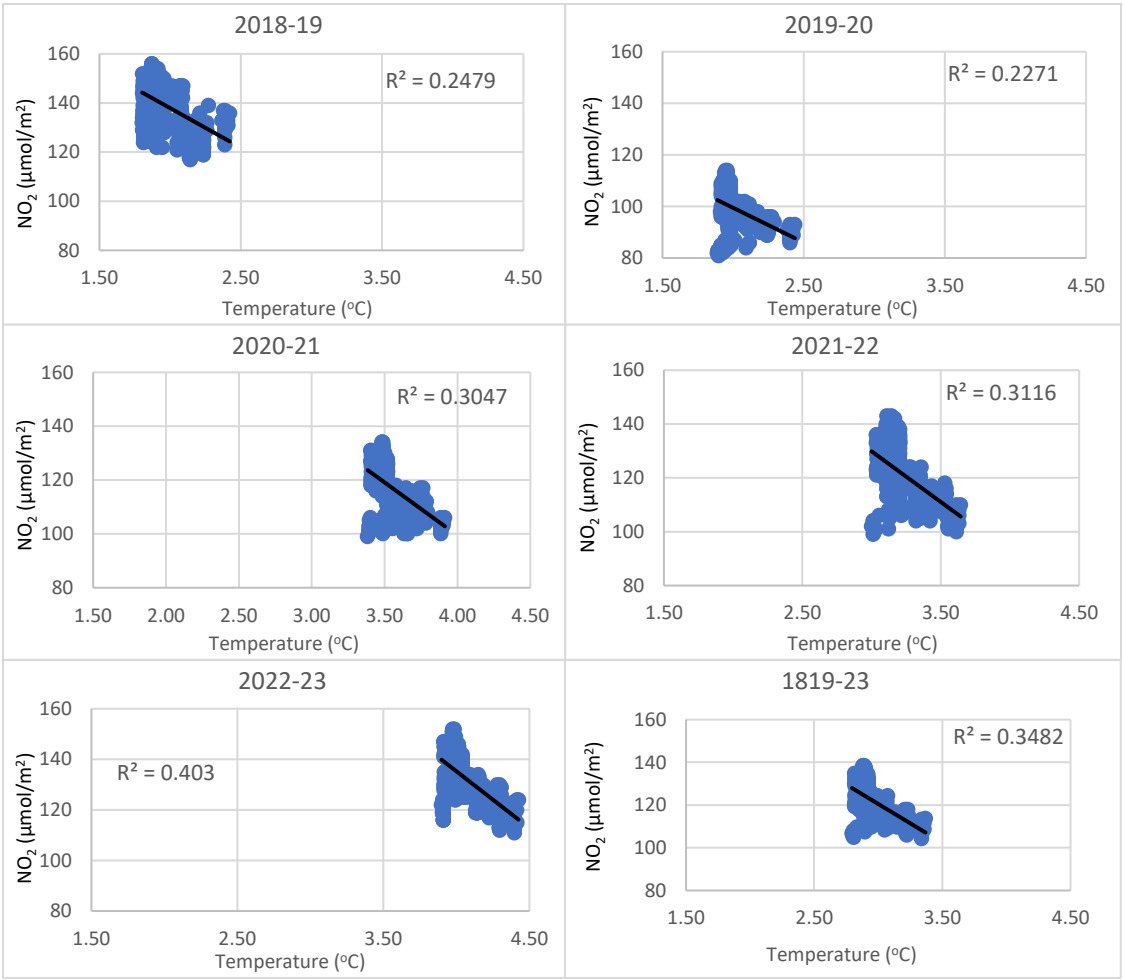

Figure 4. 13 The relationship between satellite-retrieved annual mean NO_2 and annual mean air temperature

O_3 shows a weak and inconsistent correlation with temperature (Table 4.5 and Figure 4.14). In 2018-19, temperature showed a very weak and positive correlation with O_3 concentration (Pearson's correlation 0.07), and the R^2 value ($R^2 = 0.0055$) was found negligible. In 2019-20 and 2022-23, the relationship becomes slightly negative and remains weak (Pearson's correlation -0.06 and -0.16, respectively) (Table 4.5). Also, the correlation of temperature with O_3 concentration is minimal and O_3 concentration is less influenced by temperature.

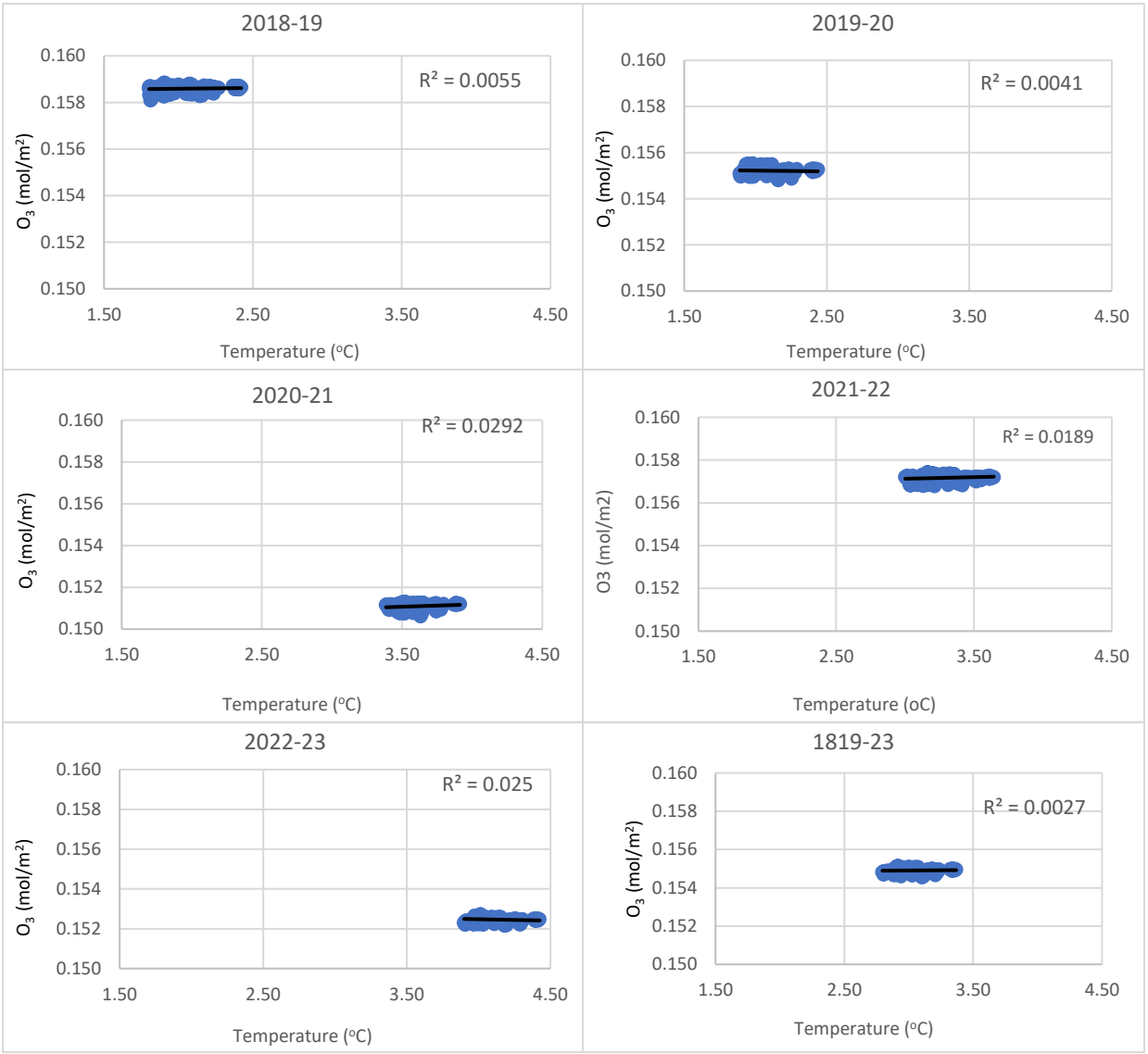

Figure 4. 14 The relationship between satellite-retrieved annual mean O_3 and annual mean air temperature

c. *Road density in relation to NO_2 and O_3*

NO_2 shows a weak but positive correlation with road density across all five years (Table 4.5 and Figure 4.15). The first two consecutive years 2018-19 and 2019-20 show a similar pattern with Pearson's correlation of 0.26, however, the following three years, 2020-21 to 2022-23, show a similar pattern but they are statistically not significant (Table 4.5 and Figure 4.15). The R^2 value is weak, varying from 0.0385 (2020-21) to 0.0664 (2019-20) (Figure 4.15), showing limited influence of road density on NO_2 concentration.

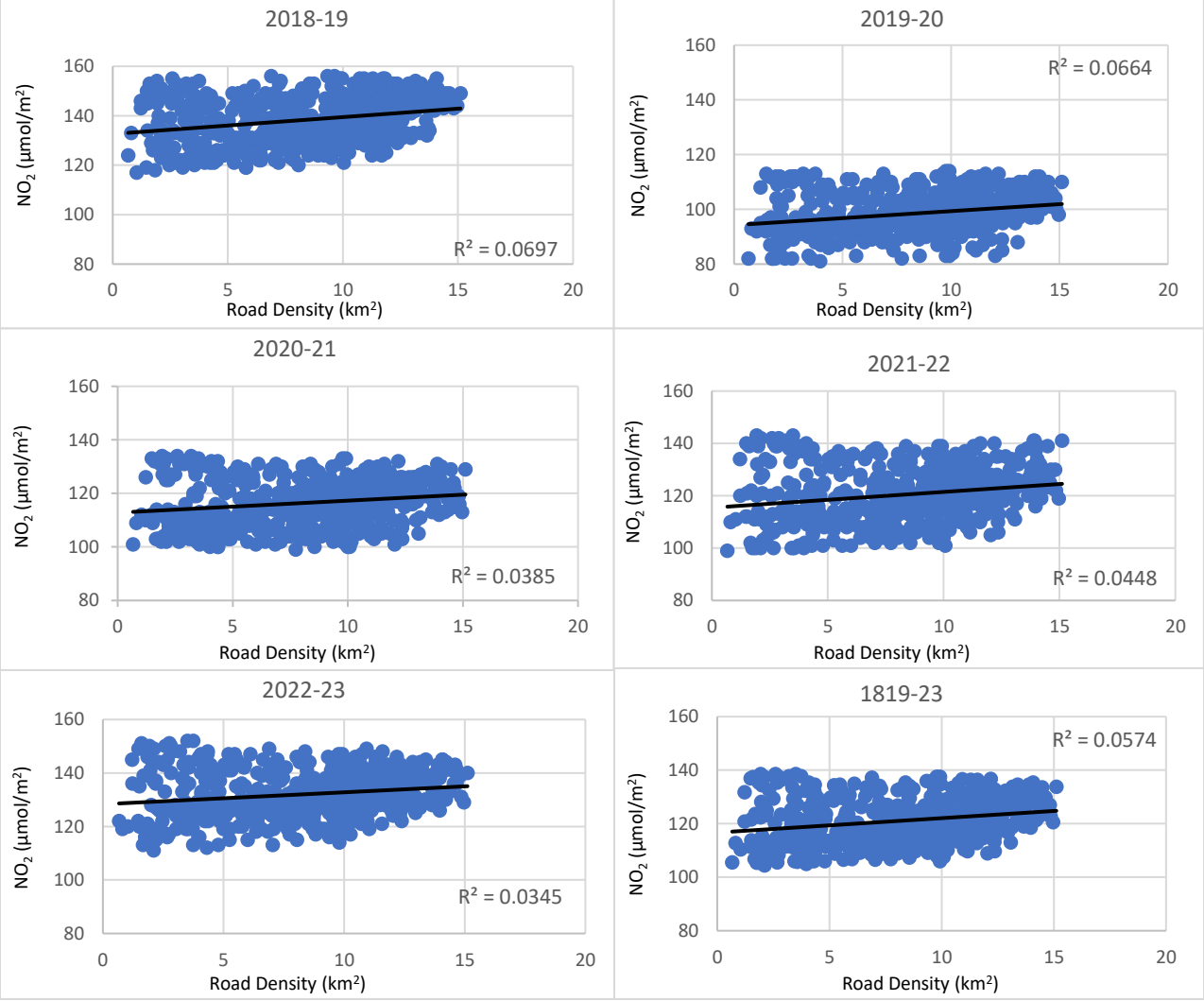

Figure 4. 15 The relationship between satellite-retrieved annual mean NO_2 and road density

O_3 shows a weak to moderate positive correlation with road density (Table 4.5 and Figure 4.16). 2018-19 and 2022-23, show a moderate relationship with Pearson's correlation of 0.41 and 0.50 respectively, and R^2 values of 0.1672 and 0.2475 respectively. Other years demonstrate a weak relationship with lower R^2 values compared to the last year 2022-23 (Figure 4.16) where 2019-20 is statistically insignificant (Table 4.5 and Figure 4.16). The relationship between O_3 and road density varies from weak to moderate over the years.

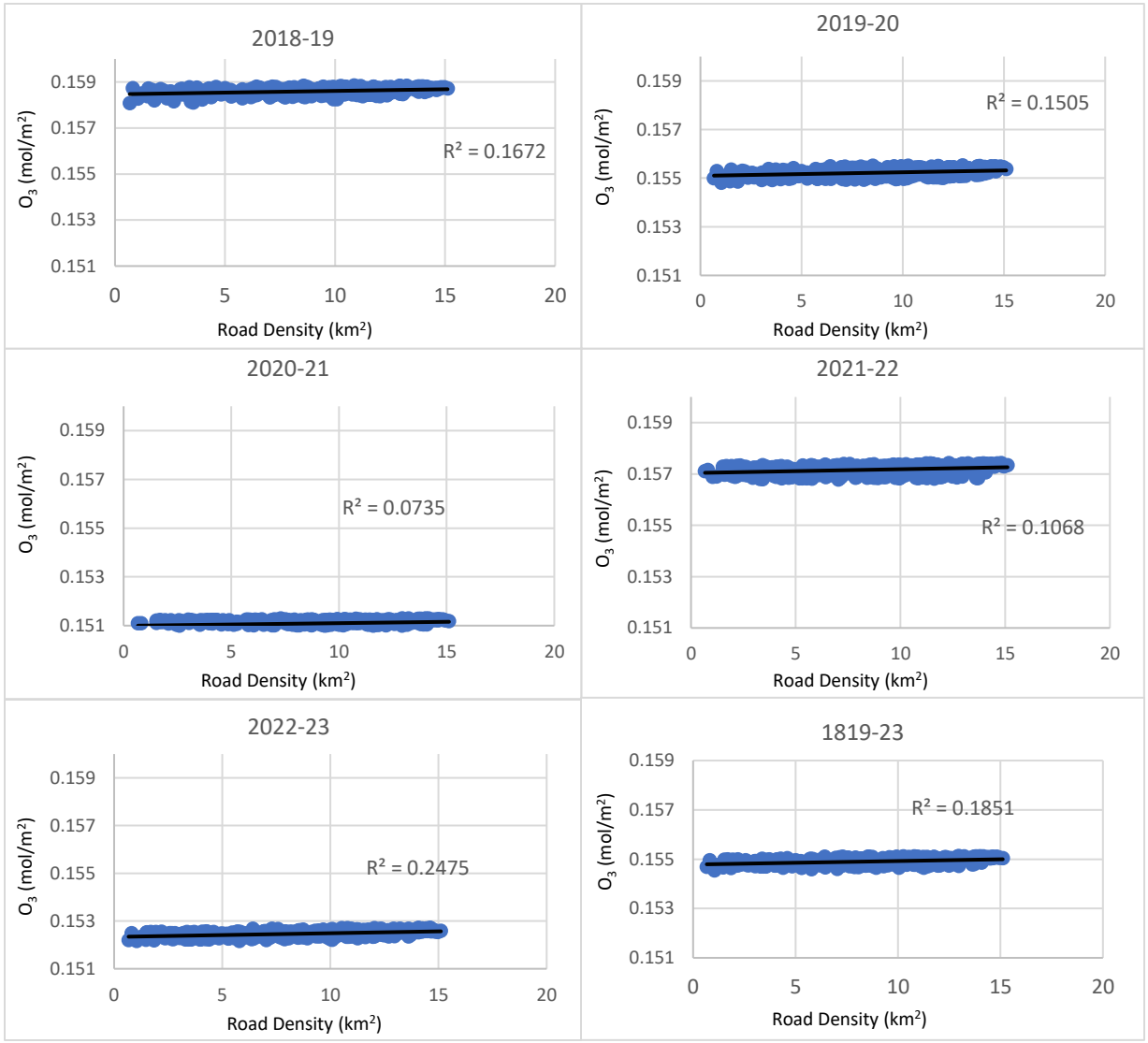

Figure 4. 16 The relationship between satellite-retrieved annual mean O_3 and road density

d. Population density in relation to NO_2 and O_3

The correlation between NO_2 and O_3 concentrations with population density for the years 2020-21 and 2021-22 shows a very weak relationship (Table 4.5 and Figure 4.17). NO_2 shows a very weak positive relationship with population density, and O_3 shows a very weak negative relationship in both 2020-21 and 2021-22 (Table 4.5). The R^2 values are negligible in both the years for NO_2 and O_3 (Figure 4.17). Also, their relationship is statistically insignificant (Table 4.5).

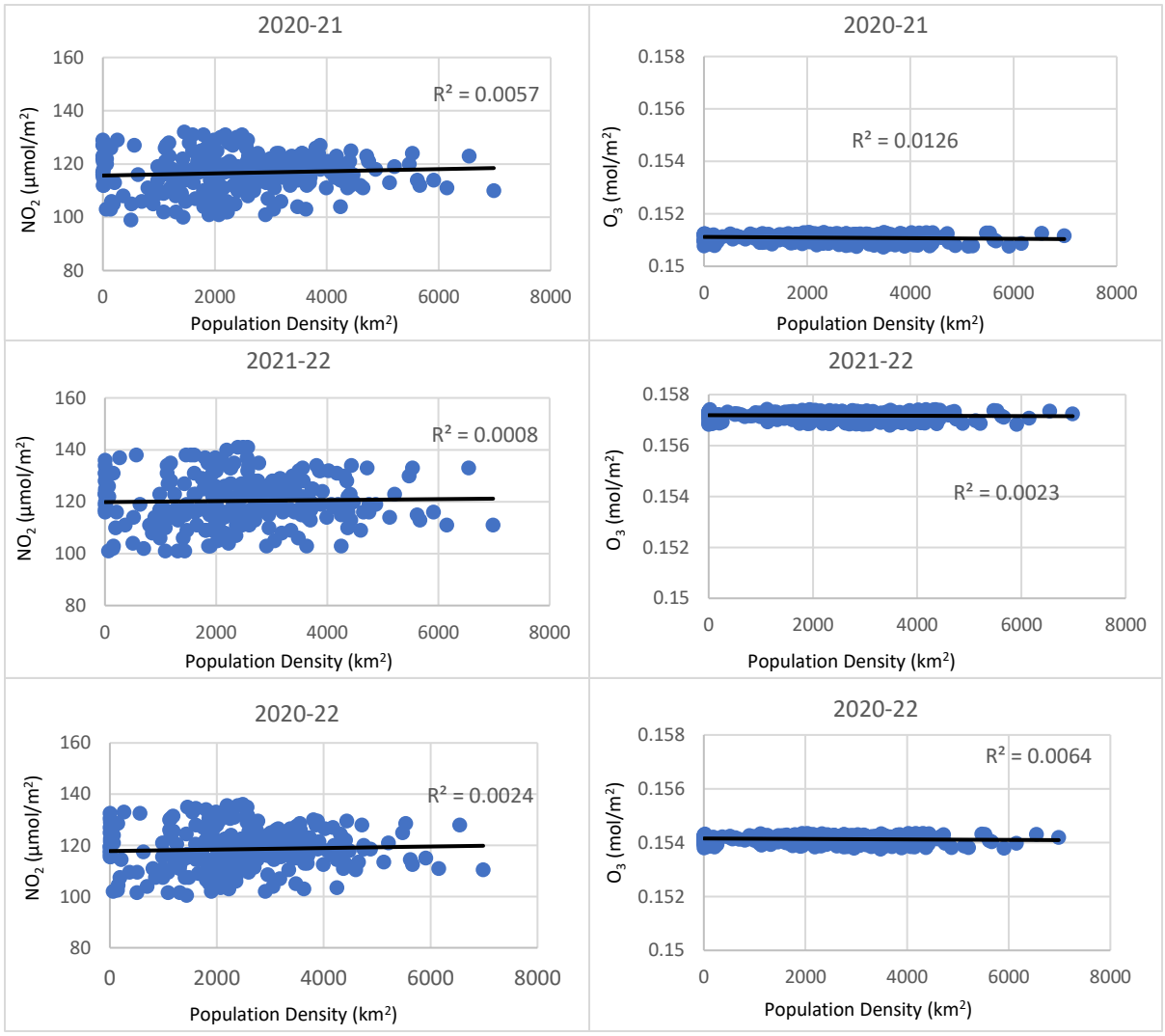

Figure 4. 17 The relationship between satellite-retrieved annual mean NO_2 and O_3 and population density (2021).

Chapter 5 Discussions

This section discusses the results of the study in three subsections: (i) patterns of NO_2 and O_3 concentration; (ii) correlations of NO_2 and O_3 with the explanatory variables (elevation, temperature, road, and population density); and (iii) data related issues.

5.1 Patterns of NO_2 and O_3

5.1.1 Temporal Patterns of NO_2 and O_3

The study finds increased NO_2 concentrations throughout the winter months (December – March) and reduced concentrations from May until November. Potential reasons for this pattern can be the increased use of fossil fuels, especially natural gas for heating throughout the winter months. The demand for heating increases, leading to more combustion of fossil fuels in residential heating systems, power plants, and industrial processes. According to the survey of household energy use in 2019, Alberta consumed 79% of energy from natural gas which is the highest percentage across Canada, 19% from electricity, and 1% from other sources (including Oil and Wood) (Natural Resources Canada, 2024). Another important reason can be the primary heating system of Edmonton. In Edmonton, 80% of primary heating systems are natural gas-based forced air furnaces and electric baseboard heaters are 4% (in 2021), while across Canada it is 51% and 25% (in 2021) respectively (Appendix A: Table A.1) (Statistics Canada, 2022b).

Traffic emissions can be another potential source that tends to be higher in winter due to the increased use of vehicles for commuting during cold weather (Pant & Harrison, 2013). Additionally, diesel engines emit more NO_2 and are more common in colder climates (Pant and Harrison 2013). Alongside, vehicles tend to run longer in cold weather, contributing to increased NO_2 concentrations (Gao et al., 2018; Grange et al., 2019). Furthermore, winter months often

experience temperature inversions, where a layer of warmer air traps pollutants like NO_2 near the ground. This phenomenon limits vertical dispersion and leads to higher concentrations at the surface level (Petetin et al., 2015; Stull, 2012).

O_3 concentration peaks during the late winter and early spring months (February to April). The intensity of primary precursors of O_3 formation, notably NO_x and Volatile Organic Compounds (VOCs) among others, may play a major role in this trend. In addition, during the winter season, consistent atmospheric conditions and temperature inversions may trap these primary pollutants near the surface and facilitate the accumulation of O_3, thus observing higher concentrations (Jacob & Winner, 2009; Jacobson, 2002; Qu et al., 2020). Furthermore, this can be intensified by lower wind speeds and reduced dispersion of air pollutants (Seinfeld & Pandis, 2016), especially in continental areas such as Edmonton. Long-range transport of pollutants at certain times of the year (typically the transition periods between seasons, such as from late winter to spring and early summer) can also contribute to higher O_3 concentrations. Pollutants emitted in one region can undergo photochemical reactions (in different layers of the atmosphere) during transport, which may lead to higher O_3 concentrations downwind (Jacob, 1999; Zhao et al., 2021).

Analyzing the weekly distribution of NO_2 and O_3, results reveal further insights into the temporal variability of these pollutants. Unsurprisingly, NO_2 concentrations are generally higher on weekdays, with the highest concentrations observed on Wednesdays and Fridays in Edmonton. This trend reflects increased vehicular traffic and industrial activities during the workweek. Conversely, NO_2 concentrations drop during weekends, particularly on Sundays, which indicates reduced emissions from these sources. In agreement with this result, Goldberg et al., 2021 describe the reduction of NO_2 concentrations during Saturday and Sunday compared to

weekdays (Goldberg et al., 2021). Other studies produce similar results such as (Beirle et al., 2003; de Foy et al., 2016; Russell et al., 2010; Wickert, 2001). One of the potential reasons for the quick daily changes can be the lifetime of NO_2 in the atmosphere, which varies roughly from a few hours to one day (Beirle et al., 2003; Leue et al., 2001). Another potential reason can be the traffic patterns and anthropogenic activity between weekends and weekdays (Goldberg et al., 2021).

O_3 exhibits less weekly variation, with relatively regular concentrations across all days. This stability suggests that O_3 formation is more influenced by longer-term atmospheric conditions, precursors availability, and chemical reactions rather than immediate changes in local-level emissions (He et al., 2021). Lal et al., (2000) finds seasonal variations in O_3 concentrations and reports higher concentrations in the daytime due to the increase in the photochemical reactions. Another study by Naja & Lal, (2002) denotes that the daylight variations in O_3 concentrations are due to the combined effect of precursor intensity, atmospheric chemistry, wind pattern, and boundary layer processes. However, the present study utilizes Sentinel-5P datasets, which provide data between 6-8 pm (Edmonton local time), this may influence the consistent pattern of O_3 concentrations. Another potential reason for the consistent pattern can be the lifetime of O_3 in the atmosphere. O_3 lifetime varies from a few hours to a few weeks and on a global scale it is approximately 22 days (Monks et al., 2015; Seinfeld & Pandis, 2016; Stevenson et al., 2006).

The first COVID-19 case was reported in January 2020 and the first presumptive case in Alberta was identified on 5th March 2020, followed by the state of emergency (SOE) in all provinces of Canada (Staff, 2022; Tian et al., 2021). During the SOE timeline, different restrictions were introduced to combat the pandemic such as movement restrictions, public

gathering restrictions, etc. (Staff, 2022). From mid-March to the end of April 2020, NO_2 shows a significant decrease in its concentration, especially in May 2020 NO_2 decreased by almost 19% compared to February 2020, potentially due to the reduced human activities, particularly in transportation and industrial sectors as highlighted by Adams, (2020), Siddiqui et al., (2022), Tian et al., (2021). Other studies have shown a similar pattern, where the COVID-19 lockdown period led to significant reductions in vehicular traffic, and vehicular traffic is known as one of the primary sources of NO_2 (Bauwens et al., 2020; M. J. Cooper et al., 2022; Fu et al., 2020). At the same time, yearly mean NO_2 patterns also suggest so, with reduced NO_2 concentration during 2019-20. The trend of increasing NO_2 in 2021-22 and 2022-23 can be partially explained by the rise in trading transportation fuels. In 2022, gasoline and diesel sales increased by 5.9% and 2.1%, respectively, from 2021 across Canada (Statistics Canada, 2023). More specifically, Ontario saw the highest increase in gasoline sales in 2022, with an 11.5% rise, followed by Alberta at 9.5% (Statistics Canada, 2023). All these are potential indicators of rising NO_2 concentrations in the post-COVID-19 period as the economy and society return to more normal operations.

5.1.2 Spatial Patterns of NO_2 and O_3:

Across all five years, areas surrounding downtown Edmonton, northeast Edmonton, and industrial areas in the southeast areas consistently saw the highest annual mean NO_2 concentration. This spatial pattern of higher concentrations of the pollutant coincides with the presence of numerous industrial facilities, such as steel and metal fabricators, glassware manufacturers, and industrial equipment producers, particularly in northwest Edmonton. Additionally, the Winterburn industrial area, an industrial District in Edmonton, may significantly contribute to the NO_2 concentrations in these regions. These regions are known for

heavy traffic as well. In addition, the southeast industrial areas, characterized by heavy industries and extensive impervious surfaces, also show elevated NO_2 concentrations. Downtown Edmonton, being a traffic hub with numerous amenities and services, further propels NO_2 concentrations, combined with the presence of sources like the Rossdale Power Plant and the use of heavy-duty generators.

Recent studies reveal that in Alberta, the upstream oil and gas industry contributes more than half of the total NO_2 emissions, whereas traffic and mobile sources are influencing the urban NO_2 concentration significantly (Government of Alberta, 2022b; Hajiparvaneh, 2023; Uarporn et al., 2018). Overall, the NO_2 spatial pattern highlights the influence of localized emissions sources and underscores the need for targeted emission reduction strategies in industrial and high-traffic areas. Although the very high NO_2 concentration area decreases in 2022-23 in terms of area covered compared to all other years, an interesting fact is that the concentration range is the same in all five studied years. Because the study utilizes the natural breaks method to classify the NO_2 concentration (Table 4.4).

The spatial distribution of O_3 presents more consistent patterns compared to NO_2 across the study period with moderate spatial variations. Central-north Edmonton, a predominantly urban and industrial area consistently receives the highest amounts of O_3 across all five years. However, the southern suburban area receives lower O_3 concentration, where traffic is lower compared to the central zone. The potential reason can be the photochemical nature of O_3 formation, which is heavily influenced by the availability of sunlight and precursor pollutants, primarily NO_2 and volatile organic compounds (VOCs) (Li et al., 2019; Sicard et al., 2020). In this case, it is important to denote that Sentinel-5P collects data during afternoon-evening time varying from ~5:30 pm to 7:30 pm (Edmonton local time) across the study area.

In the year 2022-23, O_3 concentrations decreased across the study area, with the highest concentrations centered around the decommissioned airport area that is surrounded by industries. All the other years exhibited a similar pattern. This spatial shift emphasizes the complex interplay between local emissions, meteorological conditions, availability of precursors in the atmosphere, and regional transport (O. R. Cooper et al., 2010; Sicard et al., 2020; Sillman, 1999).

5.2 Relationship with Explanatory Variables

The study finds several patterns between NO_2 concentrations and the four explanatory variables. NO_2 concentration is strongly influenced by elevation and temperature compared to road and population density. The highest correlation founds in 2018-19, and in subsequent years weakens noticeably. Though elevation plays a key role in NO_2 distribution, factors like local emissions and weather patterns may also influence NO_2 concentration significantly (Seinfeld & Pandis, 2016). On the other hand, compared to NO_2, O_3 shows an inverse strengthening relationship with elevation during the study period. This is likely due to the presence of reduced precursors such as nitrogen oxides (NO_x) and volatile organic compounds (VOCs) at higher altitudes (Li et al., 2019).

Temperature also shows a consistent and gradually increasing negative correlation with NO_2 over the study period, with similar results found as Morillas et al., (2024), and Siddiqui et al., (2022). This signifies that higher temperatures are linked to lower NO_2 concentrations. Potential reasons can be the reduced use of fossil fuel during warmer seasons, which may directly impact energy consumption, and more energy consumption triggers air pollution. Another potential reason can be the enhanced photochemical reaction that converts NO_2 into other compounds such as O_3 (Monks et al., 2015; Siddiqui et al., 2022). In contrast to NO_2, O_3 displays a weak and inconsistent relationship with temperature over the study period. This

suggests that temperature alone does not have a strong influence on O_3 concentration in the study area. In this case, temperature may influence the photochemical formation of O_3, along with the presence of other factors like the availability of precursors in the atmosphere, sunlight, etc. (Sicard et al., 2020).

The correlation between road density and NO_2 is positive but weak, which shows the impact of traffic emissions broadly. Road traffic is a significant source of NO_2, particularly in urban areas with dense road networks with intense traffic (Beirle et al., 2003). However, the present study finds a weak relationship, and the time of data captured by Sentinel-5P may play a major role here. It is expected that traffic emissions would reach their peak during office hours when Sentinel-5P collects data from 6-8 pm across the study area. In contrast to NO_2, O_3 shows a moderate positive correlation with road density, with a strengthening relationship from 2018-19 (Pearson's correlation 0.41) to 2022-23 (Pearson's correlation 0.50). This signifies the complex interaction between O_3 and NO_2 in urban-built environments, where road traffic contributes to the major precursors of O_3, which can subsequently trigger O_3 formation through photochemical reactions (Monks et al., 2015; Siddiqui et al., 2022; Sillman, 1999).

Finally, NO_2 and O_3 show very weak correlations with population density. This indicates an almost negligible influence of population density on NO_2 and O_3 concentrations in the study area and signifies that population density alone is not a strong predictor of NO_2 and O_3 fluctuations. Higher population density does not necessarily cause higher or lower O_3 concentrations, perhaps because the formation of O_3 is more dependent on the availability of precursors in the atmosphere and meteorological conditions instead of population density (Li et al., 2019; Sicard et al., 2020). Initially, it was expected that increases in the population would correlate with increasing air pollution, which could be explained by the intense use of

automobiles, per-household energy consumption, and housing industries required to build a shelter for the increased population which may significantly intensify home-hitting (Morillas et al., 2024). According to Statistics Canada and City of Edmonton projections, more than 100,000 people moved to Edmonton over the past two years. This influx drove the population up by 10%, from just over one million in 2021 to 1.14 million in 2023 (Riebe, 2024). So, further detailed investigation may help to unfold the impact of this increased population on NO_2 and O_3 concentration.

5.3 Data Limitations

Missing data and errors

The study finds an overall 10% and 1% of satellite data were missing for NO_2 and O_3, respectively over the period. The potential reasons include ground segment anomaly, Copernicus ground segment issue, fewer measurements and reduced quality, and disruptive atmospheric conditions, among others.

Spatial resolution of Sentinel-5P data

The original spatial resolution of the Sentinel-5P data is 5.5km by 3.5km (Griffin et al., 2020; Siddiqui et al., 2022), however, the study utilizes approximately 1km spatial resolution data from Google Earth Engine (GEE) (Google Earth Engine, 2024d, 2024e). While better, the approximately 1km spatial resolution data cannot identify road/street level emissions (Goldberg et al., 2021; Griffin et al., 2020) because the road width is not even equal to the spatial resolution of the satellite data. To overcome this limitation, suitable interpolation techniques may be applied to enhance the spatial resolution of the satellite data. In this case, level 2 Sentinel-5P data with its original spatial resolution (5.5km by 3.5km) should be utilized to ensure minimal data

convergence. It is important to note about the 1km spatial resolution data that GEE has not provided much information about downsampling methods such as which interpolation techniques it utilized to produce 1km pollution data.

Temporal variability

The temporal resolution of Sentinel-5P is twice a day. It collects data between 6-8 pm (Edmonton local time) and this might be one of the potential reasons for week correlation between NO_2 and road density, because higher traffic congestation occurs during office hours, typically at the morning 7am – 9am and afternoon 3pm -5pm.

Chapter 6 Concluding Remarks and Future Work

6.1 Summary

The study explains the temporal and spatial distribution of NO_2 and O_3 concentrations, and their relationship with elevation, temperature, road density, and population density across Edmonton during 2018-2023. It finds notable variations in NO_2 concentrations and relatively lower variations in O_3 concentrations in Edmonton. NO_2 significantly increases during the winter months (December to February) and decreases in the summer months (June to August). O_3 peaks in late winter and early spring (February to April) and decreases in late summer and early fall (August to October). This seasonality highlights the role of climatic factors and human activities on the behavior of air pollutants where with the increase of temperature, NO_2 decreases, while lower temperature triggers home heating and increases NO_2 levels. It also finds noteworthy daily variability, where NO_2 concentrations are generally higher on weekdays, with peaks on Wednesdays and drops during weekends, particularly on Sundays. O_3 remains stable throughout the week. Developed urban areas with higher traffic congestion and industrial areas consistently exhibit the highest NO_2 concentrations, while O_3 shows a largely inverse spatial pattern. The study identifies temperature and elevation as the most influential variable for NO_2, and elevation and road density for O_3 along with some variability across the study period.

The findings of the study may help decision-makers in many ways. Firstly, NO_2 pollution control should be prioritized in hotspot areas like central Edmonton and near major highways. Secondly, the relationship between air pollutants and explanatory variables can be utilized to prepare guidelines for urban development plans to ensure sustainable built environments. Thirdly, winter season compatible policies can be undertaken to reduce air pollution during winter months, such as promoting the use of renewable energy, introducing carpooling

initiatives, and planning for developments that are more energy efficient in both their heating system. Fourthly, the result of the study implies the need for advanced traffic management in highly dense downtown Edmonton areas, and planning for more efficient transportation infrastructure such as promoting walking among other active transport options.

6.2 Future Work

Neighborhood-level spatiotemporal analysis can be undertaken utilizing data fusion techniques where high-resolution optical remote sensing data or microwave remote sensing data could be combined with Sentinel-5P data. Using these methods, high-resolution air pollution data can be produced, and emission sources can be identified precisely employing high-resolution air pollution data.

Station-based observation data can be collected and compared with the present study. This will allow us to know more about the convenient data sources. Similarly, station data can also be utilized to conduct neighborhood-level studies by choosing small areas where the density of the station is high and using interpolation techniques to scale up the spatial resolution of the data. Neighborhood scale work can also be initiated by incorporating energy consumption data at the civic address level.

Additional explanatory variables such as wind speed, wind direction, population density, land uses, among others can be investigated to gain a better understanding of the behavior and influences of air pollutants across the study area. Sunshine hours play a major role in the cycle of NO_2 and O_3 formation (described in 2.3). Therefore, hourly or daily sunshine hours can be investigated as an explanatory variable. In this case, the relationship between hourly station data of NO_2 and O_3, and hourly sunshine data can be investigated. Socio-economic data of the census tract can also be pulled off to investigate its influence on the variability of air pollutants. Such as,

average household size, different income groups, different age group, household types, and mobility status.

The study utilizes freely available and open-source satellite and station-based air pollution data (2018-19 to 2022-23) and provides a foundation for decision-making in environmental policy for Edmonton, Canada. The data and techqnieus employed in this study can be replicated for other cities across Canada, and indeed around the globe. Doing so would provide policy makers essential insights into the distirbution of air-borne pollutants across their study areas. Epxnadoing the work would also enrich the scientific community in understanding the relationship between ozone and nitrogen dioxide concentations and the various environmental and anthropological conditions. As the world's population continues to urbanize, air pollutants including ozone and nitrogen dioxide will continue to be major issue. Effective monitoring is essential in managing and minimizing the public health issues surrounding increasing levels o nitrogen dioxide and ozone in Edmonton and beyond.

References

Adams, M. D. (2020). Air pollution in Ontario, Canada during the COVID-19 State of Emergency. *Science of the Total Environment, 742*, 140516.

Amin, M. S. R., Tamima, U., & Amador Jimenez, L. (2017). Understanding Air Pollution from Induced Traffic during and after the Construction of a New Highway: Case Study of Highway 25 in Montreal. *Journal of Advanced Transportation, 2017*(3). https://doi.org/10.1155/2017/5161308

Araújo, C. S. P. de, Silva, I. A. C. e, Ippolito, M., & Almeida, C. D. G. C. de. (2022). Evaluation of air temperature estimated by ERA5-Land reanalysis using surface data in Pernambuco, Brazil. *Environmental Monitoring and Assessment*, *194*(5), 381.

Atkinson, R. (2000). Atmospheric chemistry of VOCs and NOx. *Atmospheric Environment*, *34*(12–14), 2063–2101.

Bălă, G.-P., Râjnoveanu, R.-M., Tudorache, E., Motișan, R., & Oancea, C. (2021). Air pollution exposure—the (in) visible risk factor for respiratory diseases. *Environmental Science and Pollution Research*, *28*(16), 19615–19628.

Barbato, G., Barini, E. M., Genta, G., & Levi, R. (2011). Features and performance of some outlier detection methods. *Journal of Applied Statistics*, *38*(10), 2133–2149.

Bari, M. D., & Kindzierski, W. B. (2015). Fifteen-year trends in criteria air pollutants in oil sands communities of Alberta, Canada. *Environment International*, *74*, 200–208.

Bauwens, M., Compernolle, S., Stavrakou, T., Müller, J., Van Gent, J., Eskes, H., Levelt, P. F., Van Der A, R., Veefkind, J. P., & Vlietinck, J. (2020). Impact of coronavirus outbreak on NO2 pollution assessed using TROPOMI and OMI observations. *Geophysical Research Letters*, *47*(11), e2020GL087978.

Beirle, S., Platt, U., Wenig, M., & Wagner, T. (2003). Weekly cycle of NO 2 by GOME measurements: a signature of anthropogenic sources. *Atmospheric Chemistry and Physics*, *3*(6), 2225–2232.

Berman, J. D., & Ebisu, K. (2020). Changes in US air pollution during the COVID-19 pandemic. *Science of the Total Environment*, *739*, 139864.

Bernatsky, S., Smargiassi, A., Barnabe, C., Svenson, L. W., Brand, A., Martin, R. V, Hudson, M., Clarke, A. E., Fortin, P. R., & van Donkelaar, A. (2016). Fine particulate air pollution and systemic autoimmune rheumatic disease in two Canadian provinces. *Environmental Research*, *146*, 85–91.

Biswal, A., Singh, T., Singh, V., Ravindra, K., & Mor, S. (2020). COVID-19 lockdown and its impact on tropospheric NO2 concentrations over India using satellite-based data. *Heliyon*, *6*(9), e04764.

Bodah, B. W., Neckel, A., Maculan, L. S., Milanes, C. B., Korcelski, C., Ramírez, O., Mendez-Espinosa, J. F., Bodah, E. T., & Oliveira, M. L. S. (2022). Sentinel-5P TROPOMI satellite application for NO2 and CO studies aiming at environmental valuation. *Journal of Cleaner Production*, *357*, 131960.

Bolaji, B. O., & Huan, Z. (2013). Ozone depletion and global warming: Case for the use of natural refrigerant–a review. *Renewable and Sustainable Energy Reviews*, *18*, 49–54.

Burnett, R. T., Stieb, D., Brook, J. R., Cakmak, S., Dales, R., Raizenne, M., Vincent, R., & Dann, T. (2004). Associations between short-term changes in nitrogen dioxide and mortality in Canadian cities. *Archives of Environmental Health: An International Journal*, *59*(5), 228–236.

City of Edmonton. (2016). *Winter Design Guidelines*.

City of Edmonton. (2017). *Annual Growth Monitoring Report*.

City of Edmonton. (2023). *Geography and climate*.

Cooper, M. J., Martin, R. V, Hammer, M. S., Levelt, P. F., Veefkind, P., Lamsal, L. N., Krotkov, N. A., Brook, J. R., & McLinden, C. A. (2022). Global fine-scale changes in ambient NO2 during COVID-19 lockdowns. *Nature*, *601*(7893), 380–387.

Cooper, O. R., Parrish, D. D., Stohl, A., Trainer, M., Nédélec, P., Thouret, V., Cammas, J.-P., Oltmans, S. J., Johnson, B. J., & Tarasick, D. (2010). Increasing springtime ozone mixing ratios in the free troposphere over western North America. *Nature*, *463*(7279), 344–348.

Correaa, M., Duquec, M., Mezad, M., & Salazar, R. (2022). NO2 Correlation Using Sentinel-5P Images and on-site Measurements during the Evolution of COVID-19 and its Influence in the Metropolitan District of Quito, Ecuador. *International Journal on Advanced Science, Engineering and Information Technology*.

de Foy, B., Lu, Z., & Streets, D. G. (2016). Impacts of control strategies, the Great Recession and weekday variations on NO2 columns above North American cities. *Atmospheric Environment*, *138*, 74–86.

Debone, D., Da Costa, M. V, & Miraglia, S. G. E. K. (2020). 90 days of COVID-19 social distancing and its impacts on air quality and health in Sao Paulo, Brazil. *Sustainability*, *12*(18), 7440.

Doiron, D., Setton, E. M., Shairsingh, K., Brauer, M., Hystad, P., Ross, N. A., & Brook, J. R. (2020). Healthy built environment: Spatial patterns and relationships of multiple exposures and deprivation in Toronto, Montreal and Vancouver. *Environment International*, *143*, 106003.

ECMWF. (2024). *Advancing global NWP through international collaboration*. https://www.ecmwf.int/

Environment and Climate Change Canada. (2024). *Air Pollutant Emissions Inventory*. https://www.canada.ca/en/environment-climate-change/services/environmental-indicators/air-pollutant-emissions.html

Environmental Protection Agency. (2018). *Ground-level Ozone Pollution.* https://www.epa.gov/ground-level-ozone-pollution/ground-level-ozone-basics

Eskes, H. J., & Eichmann, K. U. (2018). *S5P mission performance centre nitrogen dioxide [L2 _ NO2_ _] readme document*. S5P-MPC-KNMI-PRF-NO2, KNMI, available at:

https://sentinel. esa. int ….

Eskes, H., van Geffen, J., Boersma, F., Eichmann, K.-U., Apituley, A., Pedergnana, M., Sneep, M., Veefkind, J. P., & Loyola, D. (2019). Sentinel-5 precursor/TROPOMI level 2 product user manual nitrogendioxide. *Ministry of Infrastructure and Water Management*.

ESRI. (2024a). *Data classification methods*. https://pro.arcgis.com/en/pro-app/latest/help/mapping/layer-properties/data-classification-methods.htm

ESRI. (2024b). *Optimized Hot Spot Analysis (Spatial Statistics)*. https://pro.arcgis.com/en/pro-app/latest/tool-reference/spatial-statistics/optimized-hot-spot-analysis.htm

European Space Agency. (2023a). *Copernicus Open Access Hub*. https://scihub.copernicus.eu/

European Space Agency. (2023b). *S5P Mission: Overview of Sentinel-5P Mission*. https://sentinel.esa.int/web/sentinel/missions/sentinel-5p

European Space Agency. (2024). *Document Library*. https://sentiwiki.copernicus.eu/web/document-library#DocumentLibrary-SENTINEL-5PDocumentsLibrary-S5P-Documents

Fu, F., Purvis-Roberts, K. L., & Williams, B. (2020). Impact of the COVID-19 pandemic lockdown on air pollution in 20 major cities around the world. *Atmosphere*, *11*(11), 1189.

Ganzeveld, L., Bouwman, L., Stehfest, E., van Vuuren, D. P., Eickhout, B., & Lelieveld, J. (2010). Impact of future land use and land cover changes on atmospheric chemistry-climate interactions. *Journal of Geophysical Research: Atmospheres*, *115*(D23).

Gao, M., Han, Z., Liu, Z., Li, M., Xin, J., Tao, Z., Li, J., Kang, J.-E., Huang, K., & Dong, X. (2018). Air quality and climate change, Topic 3 of the Model Inter-Comparison Study for Asia Phase III (MICS-Asia III)–Part 1: Overview and model evaluation. *Atmospheric Chemistry and Physics*, *18*(7), 4859–4884.

Goldberg, D. L., Anenberg, S. C., Kerr, G. H., Mohegh, A., Lu, Z., & Streets, D. G. (2021). TROPOMI NO2 in the United States: A detailed look at the annual averages, weekly cycles, effects of temperature, and correlation with surface NO2 concentrations. *Earth's Future*, *9*(4), e2020EF001665.

Google Earth Engine. (2024a). *A planetary-scale platform for Earth science data & analysis*. https://earthengine.google.com/

Google Earth Engine. (2024b). *Earth Engine Code Editor*. https://developers.google.com/earth-engine/guides/playground

Google Earth Engine. (2024c). *ERA5-Land Daily Aggregated - ECMWF Climate Reanalysis*. https://developers.google.com/earth-engine/datasets/catalog/ECMWF_ERA5_LAND_DAILY_AGGR

Google Earth Engine. (2024d). *Sentinel-5P OFFL NO2: Offline Nitrogen Dioxide*. https://developers.google.com/earth-engine/datasets/catalog/COPERNICUS_S5P_OFFL_L3_NO2

Google Earth Engine. (2024e). *Sentinel-5P OFFL O3: Offline Ozone*.

https://developers.google.com/earth-engine/datasets/catalog/COPERNICUS_S5P_OFFL_L3_O3

Goshua, A., Akdis, C. A., & Nadeau, K. C. (2022). World Health Organization global air quality guideline recommendations: executive summary. *Allergy*, *77*(7), 1955–1960.

Government of Alberta. (2022a). *Economic overview of Edmonton*. https://www.alberta.ca

Government of Alberta. (2022b). *Effects of the spring 2020 COVID-19 public health emergency on urban air quality in Alberta*.

Government of Canada. (2023). *Air pollution: drivers and impacts*. https://www.canada.ca/en/environment-climate-change/services/environmental-indicators/air-pollution-drivers-impacts.html

Grange, S. K., Farren, N. J., Vaughan, A. R., Rose, R. A., & Carslaw, D. C. (2019). Strong temperature dependence for light-duty diesel vehicle NO x emissions. *Environmental Science & Technology*, *53*(11), 6587–6596.

Granli, T., & Bockman, O. C. (1994). Processes that from N2O in soils, nitrogen oxide from agriculture. *Norwegian Journal of Agricultural Sciences*, *12*, 18–22.

Griffin, D., McLinden, C. A., Racine, J., Moran, M. D., Fioletov, V., Pavlovic, R., Mashayekhi, R., Zhao, X., & Eskes, H. (2020). Assessing the impact of corona-virus-19 on nitrogen dioxide levels over Southern Ontario, Canada. *Remote Sensing*, *12*(24), 4112.

Grzybowski, P. T., Markowicz, K. M., & Musiał, J. P. (2023). Estimations of the Ground-Level NO2 Concentrations Based on the Sentinel-5P NO2 Tropospheric Column Number Density Product. *Remote Sensing*, *15*(2), 378.

Guenther, A. (2007). "Estimates of global terrestrial isoprene emissions using MEGAN (Model of Emissions of Gases and Aerosols from Nature)" published in Atmos. Chem. Phys., 6, 3181–3210, 2006. *Atmos. Chem. Phys*, *7*, 4327.

Hajiparvaneh, E. (2023). *Sensitivity of Ambient NO2 Concentration to Upstream Oil and Gas and Transportation Emissions in Alberta* [University of Alberta]. https://doi.org/https://doi.org/10.7939/r3-4sw8-cq25

Hashim, B. M., Al-Naseri, S. K., Al-Maliki, A., & Al-Ansari, N. (2021). Impact of COVID-19 lockdown on NO2, O3, PM2. 5 and PM10 concentrations and assessing air quality changes in Baghdad, Iraq. *Science of the Total Environment*, *754*, 141978.

He, Y., Wang, H., Wang, H., Xu, X., Li, Y., & Fan, S. (2021). Meteorology and topographic influences on nocturnal ozone increase during the summertime over Shaoguan, China. *Atmospheric Environment*, *256*, 118459.

Health Canada. (2021). *Health impacts of air pollution in Canada: estimates of premature deaths and nonfatal outcomes - 2021 report*. https://www.canada.ca/en/health-canada/services/publications/healthy-living/2021-health-effects-indoor-air-pollution.html

Health Canada. (2024a). *Health impacts of air pollution in Canada in 2018*. https://www.canada.ca/en/health-canada/services/publications/healthy-living/health-

impacts-air-pollution-2018.html

Health Canada. (2024b). *Health impacts of traffic-related air pollution in Canada*. https://www.canada.ca/en/health-canada/services/publications/healthy-living/health-impacts-traffic-related-air-pollution.html

Hersbach, H., Bell, B., Berrisford, P., Hirahara, S., Horányi, A., Muñoz-Sabater, J., Nicolas, J., Peubey, C., Radu, R., & Schepers, D. (2020). The ERA5 global reanalysis. *Quarterly Journal of the Royal Meteorological Society*, *146*(730), 1999–2049.

Hossain, M. D. (2019). *Use of Google Earth engine in monitoring and analyzing wetland dynamics in Tanguar Haor, Bangladesh*. University of Twente.

Huang, G., & Sun, K. (2020). Non-negligible impacts of clean air regulations on the reduction of tropospheric NO2 over East China during the COVID-19 pandemic observed by OMI and TROPOMI. *Science of the Total Environment*, *745*, 141023.

Ialongo, I., Virta, H., Eskes, H., Hovila, J., & Douros, J. (2020). Comparison of TROPOMI/Sentinel-5 Precursor NO 2 observations with ground-based measurements in Helsinki. *Atmospheric Measurement Techniques*, *13*(1), 205–218.

IHME. (2019). *The Global Burden of Disease (GBD) Country profiles – 2017*. Institute for Health Metrics and Evaluation. http://www.healthdata.org/canada

IOWA Department of Natural Resources. (2024). *Effects of Ground Level Ozone*. https://www.iowadnr.gov/Environmental-Protection/Air-Quality/Air-Pollutants/Effects-Ozone#:~:text=Breathing ground-level ozone can,may permanently scar lung tissue.

Jacob, D. J. (1999). *Introduction to atmospheric chemistry*. Princeton university press.

Jacob, D. J., & Winner, D. A. (2009). *Effect of Climate Change on Air Quality*. *Atmos-pheric Environment, 43, 51-63*.

Jacobson, M. Z. (2002). *Atmospheric pollution: history, science, and regulation*. Cambridge University Press.

Jaffe, D. A., & Wigder, N. L. (2012). Ozone production from wildfires: A critical review. *Atmospheric Environment*, *51*, 1–10.

Jeong, U., & Hong, H. (2021). Assessment of tropospheric concentrations of NO2 from the TROPOMI/Sentinel-5 precursor for the estimation of long-term exposure to surface NO2 over South Korea. *Remote Sensing*, *13*(10), 1877.

Jewell, D. A. (2023). *Automated prediction of tailings areas at historic gold mine districts in Nova Scotia using multispectral images and a random forest classifier*.

Johnson, B. J., Jaffe, D., Stohl, A., Aikin, K., Cammas, J. P., Weinheimer, A., Gao, R., Tarasick, D., Thouret, V., & Avery, M. A. (2010). *Increasing Springtime Ozone Mixing Ratios in the Free Troposphere Over Western North America*.

Kaplan, G., Avdan, Z. Y., & Avdan, U. (2019). Spaceborne nitrogen dioxide observations from the sentinel-5P TROPOMI over Turkey. *Multidisciplinary Digital Publishing Institute Proceedings*, *18*(1), 4.

Kazemi Garajeh, M., Laneve, G., Rezaei, H., Sadeghnejad, M., Mohamadzadeh, N., & Salmani, B. (2023). Monitoring Trends of CO, NO2, SO2, and O3 Pollutants Using Time-Series Sentinel-5 Images Based on Google Earth Engine. *Pollutants*, *3*(2), 255–279.

Krivoshto, I. N., Richards, J. R., Albertson, T. E., & Derlet, R. W. (2008). The toxicity of diesel exhaust: implications for primary care. *The Journal of the American Board of Family Medicine*, *21*(1), 55–62.

Labzovskii, L. D., Jeong, S.-J., & Parazoo, N. C. (2019). Working towards confident spaceborne monitoring of carbon emissions from cities using Orbiting Carbon Observatory-2. *Remote Sensing of Environment*, *233*, 111359.

Lal, S., Naja, M., & Subbaraya, B. H. (2000). Seasonal variations in surface ozone and its precursors over an urban site in India. *Atmospheric Environment*, *34*(17), 2713–2724.

Lamsal, L. N., Martin, R. V, Parrish, D. D., & Krotkov, N. A. (2013). Scaling relationship for NO2 pollution and urban population size: a satellite perspective. *Environmental Science & Technology*, *47*(14), 7855–7861.

Lee, C. (2020). *Climate Sensitive Urban Design of Public Open Spaces for Winter Cities: Edmonton, Canada*. 서울대학교 대학원.

Leue, C., Wenig, M., Wagner, T., Klimm, O., Platt, U., & Jähne, B. (2001). Quantitative analysis of NO x emissions from Global Ozone Monitoring Experiment satellite image sequences. *Journal of Geophysical Research: Atmospheres*, *106*(D6), 5493–5505.

Li, K., Jacob, D. J., Liao, H., Shen, L., Zhang, Q., & Bates, K. H. (2019). Anthropogenic drivers of 2013–2017 trends in summer surface ozone in China. *Proceedings of the National Academy of Sciences*, *116*(2), 422–427.

Liu, J., Hagan, D. F. T., & Liu, Y. (2020). Global land surface temperature change (2003–2017) and its relationship with climate drivers: AIRS, MODIS, and ERA5-land based analysis. *Remote Sensing*, *13*(1), 44.

Liu, R. E., Ravikumar, A. P., Bi, X. T., Zhang, S., Nie, Y., Brandt, A., & Bergerson, J. A. (2021). Greenhouse gas emissions of western Canadian natural gas: proposed emissions tracking for life cycle modeling. *Environmental Science & Technology*, *55*(14), 9711–9720.

Lu, Q.-B. (2022). Observation of large and all-season ozone losses over the tropics. *AIP Advances*, *12*(7), 75006.

McNicholl, B., Lee, Y. H., Campbell, A. G., & Dev, S. (2021). Evaluating the reliability of air temperature from ERA5 reanalysis data. *IEEE Geoscience and Remote Sensing Letters*, *19*, 1–5.

Monks, P. S., Archibald, A. T., Colette, A., Cooper, O., Coyle, M., Derwent, R., Fowler, D., Granier, C., Law, K. S., & Mills, G. E. (2015). Tropospheric ozone and its precursors from the urban to the global scale from air quality to short-lived climate forcer. *Atmospheric Chemistry and Physics*, *15*(15), 8889–8973.

Moore, D. S., McCabe, G. P., & Craig, B. A. (2009). *Introduction to the Practice of Statistics* (Vol. 4). WH Freeman New York.

Morillas, C., Alvarez, S., Pires, J. C. M., Garcia, A. J., & Martinez, S. (2024). Impact of the implementation of Madrid's low emission zone on NO2 concentration using Sentinel-5P/TROPOMI data. *Atmospheric Environment, 320*, 120326.

Müller, I., Erbertseder, T., & Taubenböck, H. (2022). Tropospheric NO2: Explorative analyses of spatial variability and impact factors. *Remote Sensing of Environment, 270*, 112839.

Muller, M. J. (2012). *Selected climatic data for a global set of standard stations for vegetation science* (Vol. 5). Springer Science & Business Media.

Muñoz Sabater, J. (2019). *ERA5-Land monthly averaged data from 1981 to present, Copernicus Climate Change Service (C3S) Climate Data Store (CDS)[Accessed on March 26, 2024]*. https://doi.org/doi:10.24381/cds.68d2bb30

Naeger, A. R., & Murphy, K. (2020). Impact of COVID-19 containment measures on air pollution in California. *Aerosol and Air Quality Research*, *20*(10), 2025–2034.

Naeimi, G. (2021). *Assessment of drought impacts on groundwater table in the Netherlands using gridded datasets in Google Earth Engine (GEE)*. University of Twente, Netherlands.

Naja, M., & Lal, S. (2002). Surface ozone and precursor gases at Gadanki (13.5 N, 79.2 E), a tropical rural site in India. *Journal of Geophysical Research: Atmospheres*, *107*(D14), ACH-8.

NASA. (2024). *Giovanni*. https://giovanni.gsfc.nasa.gov/giovanni/

National Institute of Environmental Health Sciences. (2023). *Air Pollution and Your Health*. https://www.niehs.nih.gov/health/topics/agents/air-pollution/index.cfm

National Park Service. (2024). *Ozone Effects on Plants*. https://www.nps.gov/subjects/air/nature-ozone.htm

Natural Resources Canada. (2022). *Making Home Heating More Affordable for Canadians While Fighting Climate Change*. https://www.canada.ca/en/natural-resources-canada/news/2022/11/making-home-heating-more-affordable-for-canadians-while-fighting-climate-change.html

Natural Resources Canada. (2023). *High Resolution Digital Elevation Model (HRDEM) - CanElevation Series*. http://open.canada.ca/en/open-government-licence-canada

Natural Resources Canada. (2024). *Survey of Household Energy Use, 2019*. https://oee.nrcan.gc.ca/publications/statistics/sheu/2019/index.cfm#:~:text=Natural gas was the most,362.7 million GJ (50%25)

Oiamo, T. H., Luginaah, I. N., Buzzelli, M., Tang, K., Xu, X., Brook, J. R., & Johnson, M. (2012). Assessing the spatial distribution of nitrogen dioxide in London, Ontario. *Journal of the Air & Waste Management Association*, *62*(11), 1335–1345.

Pant, P., & Harrison, R. M. (2013). Estimation of the contribution of road traffic emissions to particulate matter concentrations from field measurements: A review. *Atmospheric Environment, 77*, 78–97.

Park, H., Jeong, S., Park, H., Labzovskii, L. D., & Bowman, K. W. (2021). An assessment of

emission characteristics of Northern Hemisphere cities using spaceborne observations of CO2, CO, and NO2. *Remote Sensing of Environment*, *254*, 112246.

Petetin, H., Beekmann, M., Colomb, A., Denier van der Gon, H. A. C., Dupont, J.-C., Honoré, C., Michoud, V., Morille, Y., Perrussel, O., & Schwarzenboeck, A. (2015). Evaluating BC and NO x emission inventories for the Paris region from MEGAPOLI aircraft measurements. *Atmospheric Chemistry and Physics*, *15*(17), 9799–9818.

Pilegaard, K. (2013). Processes regulating nitric oxide emissions from soils. *Philosophical Transactions of the Royal Society B: Biological Sciences*, *368*(1621), 20130126.

Pinault, L., Crouse, D., Jerrett, M., Brauer, M., & Tjepkema, M. (2016). Spatial associations between socioeconomic groups and NO2 air pollution exposure within three large Canadian cities. *Environmental Research*, *147*, 373–382.

Powell, J. M. (1978). Climatic classifications of the prairie provinces of Canada. *Essays on Meteorology and Climatology*, 211–229.

Qu, Z., Henze, D. K., Cooper, O. R., & Neu, J. L. (2020). Impacts of global NO x inversions on NO 2 and ozone simulations. *Atmospheric Chemistry and Physics*, *20*(21), 13109–13130.

Rashidi, T. H., Kanaroglou, P., Toop, E., Maoh, H., & Liu, X. (2015). Emissions and built form–an analysis of six Canadian cities. *Transportation Letters*, *7*(2), 80–91.

Riebe, N. (2024, March 7). Edmonton's population is booming and one city councillor wonders if we're ready. *CBC News*. https://www.cbc.ca/news/canada/edmonton/edmonton-s-population-is-booming-and-one-city-councillor-wonders-if-we-re-ready-1.7136203

Russell, A. R., Valin, L. C., Bucsela, E. J., Wenig, M. O., & Cohen, R. C. (2010). Space-based constraints on spatial and temporal patterns of NO x emissions in California, 2005− 2008. *Environmental Science & Technology*, *44*(9), 3608–3615.

Schneider, P., Hamer, P. D., Kylling, A., Shetty, S., & Stebel, K. (2021). Spatiotemporal patterns in data availability of the sentinel-5p no2 product over urban areas in Norway. *Remote Sensing*, *13*(11), 2095.

Schneider, S. R., Lee, K., Santos, G., & Abbatt, J. P. D. (2021). Air quality data approach for defining wildfire influence: Impacts on PM2. 5, NO2, CO, and O3 in Western Canadian cities. *Environmental Science & Technology*, *55*(20), 13709–13717.

Schumann, U., & Huntrieser, H. (2007). The global lightning-induced nitrogen oxides source. *Atmospheric Chemistry and Physics*, *7*(14), 3823–3907.

Seinfeld, J. H., & Pandis, S. N. (2016). *Atmospheric chemistry and physics: from air pollution to climate change*. John Wiley & Sons.

Shami, S., Ranjgar, B., Bian, J., Khoshlahjeh Azar, M., Moghimi, A., Amani, M., & Naboureh, A. (2022). Trends of CO and NO2 Pollutants in Iran during COVID-19 pandemic using Timeseries Sentinel-5 images in Google Earth Engine. *Pollutants*, *2*(2), 156–171.

Shehzad, K., Sarfraz, M., & Shah, S. G. M. (2020). The impact of COVID-19 as a necessary evil on air pollution in India during the lockdown. *Environmental Pollution*, *266*, 115080.

Shikwambana, L., Mhangara, P., & Mbatha, N. (2020). Trend analysis and first time observations of sulphur dioxide and nitrogen dioxide in South Africa using TROPOMI/Sentinel-5 P data. *International Journal of Applied Earth Observation and Geoinformation*, *91*, 102130.

Shin, H. H., Owen, J., Maquiling, A., Parajuli, R. P., & Smith-Doiron, M. (2022). Circulatory health risks from additive multi-pollutant models: short-term exposure to three common air pollutants in Canada. *Environmental Science and Pollution Research*, 1–16.

Sicard, P., De Marco, A., Agathokleous, E., Feng, Z., Xu, X., Paoletti, E., Rodriguez, J. J. D., & Calatayud, V. (2020). Amplified ozone pollution in cities during the COVID-19 lockdown. *Science of the Total Environment*, *735*, 139542.

Siddiqui, A., Chauhan, P., Halder, S., Devadas, V., & Kumar, P. (2022). Effect of COVID-19-induced lockdown on NO2 pollution using TROPOMI and ground-based CPCB observations in Delhi NCR, India. *Environmental Monitoring and Assessment*, *194*(10), 714.

Sillman, S. (1999). The relation between ozone, NOx and hydrocarbons in urban and polluted rural environments. *Atmospheric Environment*, *33*(12), 1821–1845.

Spurr, R., Loyola, D., Roozendael, M. Van, & Lerot, C. (2021). S5P/TROPOMI Total Ozone ATBD. *Dtsch. Zent. Für Luft Und Raumfahrt*, *67*, 535.

Staff, N. (2022, March 15). Two years of COVID-19: A timeline of the pandemic in Alberta. *Calgery Herald*. https://calgaryherald.com/news/local-news/two-years-of-covid-19-a-timeline-of-the-pandemic-in-alberta

Statistics Canada. (2021). *2021 Census – Road network file*. https://www12.statcan.gc.ca/census-recensement/2021/geo/sip-pis/rnf-frr/index2021-eng.cfm?year=21

Statistics Canada. (2022a). *Census Profile. 2021. Statistics Canada, Catalogue no. 98-316-X2021001. Ottawa. Released February 9, 2022*. https://www12.statcan.gc.ca/census-recensement/2021/dp-pd/prof/index.cfm?Lang=E (Accessed on 16 February 2023)

Statistics Canada. (2022b). *Table 38-10-0286-01 Primary heating systems and type of energy*. https://doi.org/https://doi.org/10.25318/3810028601-eng

Statistics Canada. (2023). *Table 23-10-0066-01 Sales of fuel used for road motor vehicles, annual (x 1,000)*. https://doi.org/https://doi.org/10.25318/2310006601-eng

Stevenson, D. S., Dentener, F. J., Schultz, M. G., Ellingsen, K., Van Noije, T. P. C., Wild, O., Zeng, G., Amann, M., Atherton, C. S., & Bell, N. (2006). Multimodel ensemble simulations of present-day and near-future tropospheric ozone. *Journal of Geophysical Research: Atmospheres*, *111*(D8).

Stull, R. B. (2012). *An introduction to boundary layer meteorology* (Vol. 13). Springer Science & Business Media.

Szyszkowicz, M., Thomson, E. M., de Angelis, N., Lavoie, C., & Nguyễn, T. C. (2022). Urban air pollution and emergency department visits for injury in Edmonton and Toronto, Canada. *Hygiene and Environmental Health Advances*, *4*, 100020.

Tian, X., An, C., Chen, Z., & Tian, Z. (2021). Assessing the impact of COVID-19 pandemic on urban transportation and air quality in Canada. *Science of the Total Environment*, *765*, 144270.

Uarporn, N., Jeremiah, J., Tejas, S., Pradeepa, V., Marcus, T., & Ralph, M. (2018). *Provincial Air Quality Photochemical Modelling*.

Valacchi, G., Pagnin, E., Corbacho, A. M., Olano, E., Davis, P. A., Packer, L., & Cross, C. E. (2004). In vivo ozone exposure induces antioxidant/stress-related responses in murine lung and skin. *Free Radical Biology and Medicine*, *36*(5), 673–681.

Van Geffen, J., Eskes, H. J., Boersma, K. F., Maasakkers, J. D., & Veefkind, J. P. (2019). TROPOMI ATBD of the total and tropospheric NO2 data products. *DLR Document*.

Vanos, J. K., Cakmak, S., Kalkstein, L. S., & Yagouti, A. (2015). Association of weather and air pollution interactions on daily mortality in 12 Canadian cities. *Air Quality, Atmosphere & Health*, *8*, 307–320.

Wallington, T. J., Anderson, J. E., Dolan, R. H., & Winkler, S. L. (2022). Vehicle emissions and urban air quality: 60 years of progress. *Atmosphere*, *13*(5), 650.

Wang, Y., Yuan, Q., Li, T., Tan, S., & Zhang, L. (2021). Full-coverage spatiotemporal mapping of ambient PM2. 5 and PM10 over China from Sentinel-5P and assimilated datasets: Considering the precursors and chemical compositions. *Science of The Total Environment*, *793*, 148535.

Wickert, B. (2001). Berechnung anthropogener Emissionen in Deutschland für Ozonsimulationen. In *Institut für Energiewirtschaft und Rationelle Energieanwendung. Stuttgart, Universität Stuttgart*.

Wieczorek, B. (2023). Air Pollution Patterns Mapping of SO2, NO2, and CO Derived from TROPOMI over Central-East Europe. *Remote Sensing*, *15*(6), 1565.

World Health Organization. (2021). *Ambient air pollution: Health impacts*. https://www.who.int/airpollution/ambient/health-impacts/en/ (Accessed on 4 March 2022)

World Health Organization. (2024). *Air pollution*. https://www.who.int/health-topics/air-pollution#tab=tab_1

Wu, X., Nethery, R. C., Sabath, M. B., Braun, D., & Dominici, F. (2020). Air pollution and COVID-19 mortality in the United States: Strengths and limitations of an ecological regression analysis. *Science Advances*, *6*(45), eabd4049.

Zhao, Q., He, Q., Jin, L., & Wang, J. (2021). Potential source regions and transportation pathways of reactive gases at a regional background site in northwestern China. *Advances in Meteorology*, *2021*(1), 9933466.

Appendix A

Table A. 1 An overall scenario of primary heating practices in residential heating systems over Edmonton, Alberta, and Canada (Statistics Canada, 2022b)

Primary heating systems	Edmonton			Alberta			Canada		
	2017	**2019**	**2021**	**2017**	**2019**	**2021**	**2017**	**2019**	**2021**
	Percentage								
All primary heating systems	99	99	99	99	99	99	95	95	93
Forced air furnace	***86***	***78***	***80***	***85***	***81***	***82***	***55***	***52***	***51***
Electric baseboard heaters	F	F	4	3E	3	4	26	26	25
Heating stove	F	F	F	F	F		3	2	2
Boiler with hot water or steam radiators	9	14	9	9	11	9	8	9	8
Electric radiant heating	F	F	F	F	2E	2	1	3	4
Heat pump	F	F	F	F	F	F	4	5	6
Other types of heating system	F	F	F	F	2E	2E	0	3	4

Note: E= use with caution & F= too unreliable to be published